A HIGH BANDWIDTH NON-DESTRUCTIVE METHOD FOR CHARACTERIZING SIMPLE MEDIA

THESIS

Matthew L. Szuster, Second Lieutenant, USAF

AFIT/GE/ENG/12-39

DEPARTMENT OF THE AIR FORCE
AIR UNIVERSITY

AIR FORCE INSTITUTE OF TECHNOLOGY

Wright-Patterson Air Force Base, Ohio

AFIT/GE/ENG/12-39

A HIGH BANDWIDTH NON-DESTRUCTIVE METHOD FOR CHARACTERIZING SIMPLE MEDIA

THESIS

Presented to the Faculty

Department of Electrical and Computer Engineering

Graduate School of Engineering and Management

Air Force Institute of Technology

Air University

Air Education and Training Command

In Partial Fulfillment of the Requirements for the

Degree of Master of Science in Electrical Engineering

Matthew L. Szuster, BS

Second Lieutenant, USAF

March 2012

AFIT/GE/ENG/12-39

A HIGH BANDWIDTH NON-DESTRUCTIVE METHOD FOR CHARACTERIZING SIMPLE MEDIA

Matthew L. Szuster, BS
Second Lieutenant, USAF

Approved:

Michael Havrilla Dr. Michael Havrilla (Chairman)	24 Feb 2012 Date
Milo Hyde, Major, USAF (Member)	24 Feb 2012 Date
Dr. Michael Saville (Member)	24 Feb 2012 Date

Abstract

The relative complex permittivity can be extracted with time domain data from a perfect electrical conductor (PEC) backed sample of a low-loss, non-dispersive dielectric using dual ridged waveguide aperture probes with attached PEC flange plates of the same geometry and different dimensions. The temporal domain measurement of interest is the ability to detect the reflection from the edge of the flange plate in the parallel region created by the flange plate and the PEC backing on the dielectric sample. Signal processing windows are applied to the data in order to exploit this edge reflection. The types of signal processing methods used and the geometry and size of the flange plate help identify the edge reflection.

Measurements are taken using square and circular flange plates of different dimensions. Measured data is then processing using Kaiser and Blackman-Harris windows to show the edge reflection. A simple extraction technique for the permittivity is used and compared with industry standard values.

Table of Contents

Page

List of Figures

List of Tables

Page

A High Bandwidth Non-Destructive Method for Characterizing Simple Media

I. Introduction

The world is filled with various forces that behave and interact with objects based on its material characteristics. Of particular interest are the forces related to the field of electromagnetics. Electromagnetic waves propagate and interact with materials to create conduction, magnetization, and polarization currents. The currents or forces created are related to conductivity, permeability, and permittivity. The way these electromagnetic forces interact with these currents give rise to these parameters which describe their relationships.

By understanding these parameters, the electromagnetic forces can be used to create new technology. However, the characteristics of a given material must be known within a certain range before they can be used in various applications. Various techniques have been created in order to obtain the permittivity and permeability of a material. However, these techniques prove to be computationally intensive and/or destructive to the material. The destruction of a test material and the length of time needed to extract these parameters can be costly. A method that can provide these parameters in a non-destructive and computationally simple manner could significantly decrease cost. However, such methods need to provide at least one parameter to a specified tolerance. By finding even one parameter such as permittivity, the method would be able to cut cost and avoid complexity in the extraction process.

Problem Statement

To characterize the parameters of a material, most methods require intensive computation or the destruction (i.e. machining) of the material. In order to reduce computation, a closed form solution is often sought and developed to measure either permittivity or permeability. One of the most used methods for extracting permittivity and permeability is the Nicholson Ross Weir (NRW) method [6]. In rectangular waveguide applications, the test material has to be machined or destroyed and subsequently placed in the waveguide fixture in order to measure the forward and reverse scattering parameters. There are two main problems with this method. A small sample size needs to be machined for testing which in turn means a potentially small proportion of the overall material is actually measured and validated.

Previous work has been done to create a computationally efficient, non-destructive method to characterize simple media using a time domain technique [12]. An improved method investigated in this research will measure reflections from the aperture and edges of a flanged double ridged rectangular waveguide to extract the complex permittivity of a conductor backed simple dielectric material as show in Figure 1. The improved technique will use the wider frequency range available to observe a more accurate reflection in the time domain as well as signal processing techniques to observe the reflections. In addition, the enhanced temporal resolution will allow the overall test device (i.e. flange plate) to be significantly reduced in size, leading to improved agility in non-destructive measurement scenarios.

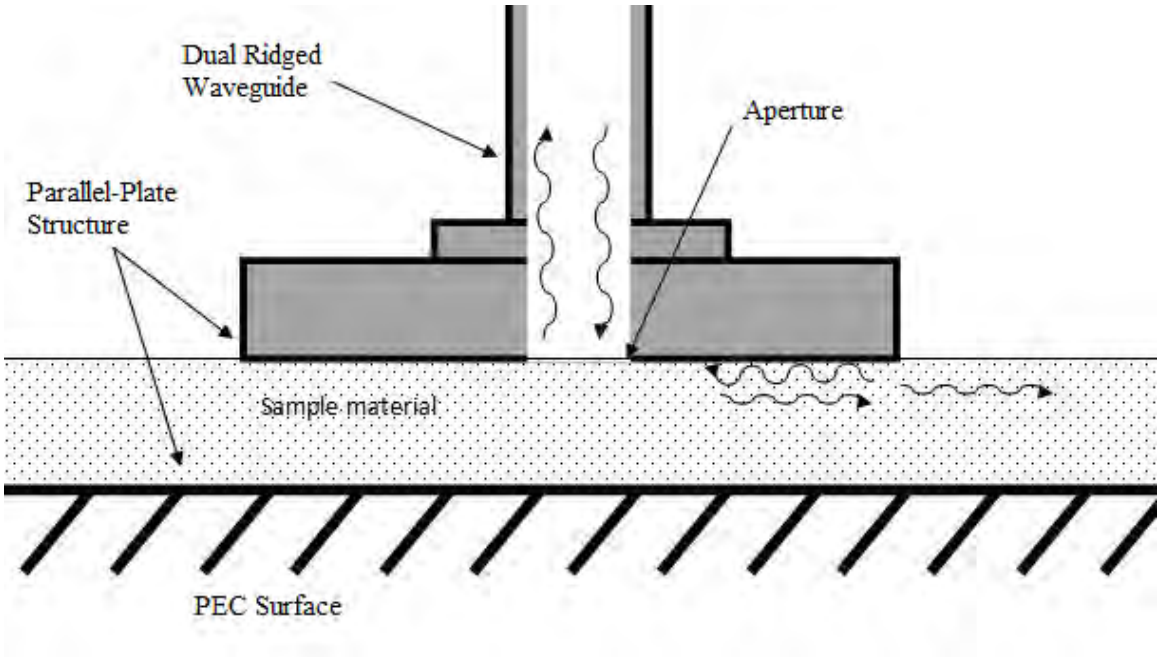

Figure 1: Basic setup of probe

Limitations

Since measurements will be taken using reflections from the edge of plates, the dielectric material must be low loss so that a reflection does, indeed, appear. Also the dielectric material must have very low dispersion; otherwise the temporal response will have low resolution. Another factor is the way the network analyzer (NWA) calculates the temporal response. The NWA does not take pulsed time domain measurements; it takes swept frequency domain measurements which are then converted to the temporal domain through the inverse fast Fourier transform (IFFT). The resolution of the time domain measurements is proportional to the inverse of the measurement frequency.

The technique used to characterize the material only uses reflection measurements. Therefore, the amount of parameters to be extracted must equal the number of measurements taken. In this case, only the complex permittivity will be solved

due to the number of reflection measurements performed. Thus, the material samples considered in this research are assumed to be non magnetic (i.e. $\mu = \mu_0$).

Scope

There are many different methods that use various probes to measure the constitutive parameters of a material. In the method presented in this research, the focus will be on using waveguides as probes. As previously mentioned, the bandwidth limits the resolution of the reflection observation in the time domain. A dual ridged rectangular waveguide will be used as a probe for measurement. This selection is based on the fact that the NWA used in this research is able to perform measurements from 10.0 MHz to 20.0 GHz. A dual ridged rectangular waveguide is able to provide significantly better coupling than a coaxial probe and has a wider bandwidth than a standard rectangular waveguide. Since the extracted parameter will be permittivity, the material under test must be non-magnetic. It is also assumed that the material has low dispersion. The computation involved to extract the parameters of the tested material does not have any other limitations in relation to the bandwidth of the probe.

The technique used to characterize the material only uses reflection measurements. Therefore, the amount of parameters to be extracted must equal the number of measurements taken. In this case, only the complex permittivity will be solved due to the number of reflection measurements performed.

Thesis Organization

Chapter 2 will provide a general background with Maxwell's equations and the related constitutive parameters that will describe what simple media is. It will also

provide the behavior of electromagnetic waves in a dual ridged waveguide, parallel plate waveguide and the process of extracting complex permittivity. Chapter 3 will describe the experimental setup, details on how calibration is performed, a calculation of the frequency bandwidth available from the dual ridged waveguide, and the data processing involved for computing the dielectric properties of the test material. Chapter 4 discusses the accuracy of the measurement method, compares raw and processed data from reflection measurement and data processing, and then computes the complex value of permittivity, which is compared to industry standards. Chapter 5 covers the conclusions of the various steps of method and presents possible future work.

II. Background

The setup in this research involves a dual ridged waveguide coupled with a dielectric filled parallel plate waveguide structure as shown in Figure 1. Maxwell's equations are first reviewed to define permittivity and formulated to be used in the parameter extraction. Next, a brief formulation of the behavior of waves in a parallel waveguide is presented, as well as an approximate technique for extracting the complex permittivity. Then, an analysis of the fields in the dual ridged waveguide is required in order to formulate equations that describe mode frequencies of the waveguide. Lastly, the major points of the chapter will be reviewed.

Maxwell's Equations and Constitutive Parameters

The relations of electric and magnetic fields, charges, and currents associated with electromagnetic waves are defined by physical laws, which are known as Maxwell's equations. The following derivations are based on Balanis [3] and Harrington [9]. Maxwell's Equations in differential form, written with an assumed and suppressed $e^{j\omega t}$ time dependence are

$$\nabla \times \vec{E} = -\vec{M_i} - j\omega\vec{B} \tag{1}$$

$$\nabla \times \vec{H} = \vec{J_i} + \vec{J_c} + j\omega\vec{D} \tag{2}$$

$$\nabla \bullet \vec{D} = q_{ev} \tag{3}$$

$$\nabla \bullet \vec{B} = q_{mv} \tag{4}$$

where $\vec{E}$ is the electric field intensity, $\vec{H}$ is the magnetic field intensity, $\vec{D}$ is the electric flux density, $\vec{B}$ is the magnetic flux density, $\vec{J}$ is the electric current density, and $\vec{M}$ is

the equivalent magnetic current density. The "i" subscript denotes an impressed current density while the "c" subscript denotes a conduction current density. Also, q_{ev} is the electric charge density and q_{mv} is the equivalent magnetic charge density.

The scope of the research limits the material to be measured as simple media, which is linear, homogeneous, and isotropic. The constitutive relations simplify to the following

$$\vec{D}(\vec{r},\omega) = \varepsilon(\omega)\vec{E}(\vec{r},\omega) \tag{5}$$

$$\vec{B}(\vec{r},\omega) = \mu(\omega)\vec{H}(\vec{r},\omega) \tag{6}$$

$$\vec{J_c}(\vec{r},\omega) = \sigma(\omega)\vec{E}(\vec{r},\omega) \tag{7}$$

As previously mentioned, the material under test has the following limitations: low loss ($\varepsilon'' \ll \varepsilon'$), non-magnetic ($\mu(\omega) \to \mu_0$), and low dispersive ($\varepsilon(\omega) \to \varepsilon$). By applying these conditions and appropriately substituting into Maxwell's equations, the complex permittivity can be derived as follows

$$\begin{aligned} \nabla \times \vec{H} &= \vec{J_i} + \sigma\vec{E} + j\omega\varepsilon\vec{E} \\ &= \vec{J_i} + j\omega\left(\varepsilon + \frac{\sigma}{j\omega}\right)\vec{E} \end{aligned} \tag{8}$$

$$\begin{aligned} \varepsilon_c &= \left(\varepsilon - j\frac{\sigma}{\omega}\right) \\ &= \varepsilon_0(\varepsilon' - j\varepsilon''). \end{aligned} \tag{9}$$

Parallel Plate Region Wave Behavior

The transverse fields inside the parallel plate region can be found by replacing the waveguide aperture with a magnetic surface current based upon Love's equivalence

principle [8]. The transverse magnetic field is found by solving the following equation [3]

$$\vec{H}_t^{pp} = \frac{1}{j\omega\varepsilon\mu}(k^2 + \nabla_t \nabla \bullet)\vec{F} \tag{10}$$

where ∇_t is the transverse gradient operator. The electric vector potential $\vec{F}$ is

$$\vec{F} = \int_0^b \int_0^a \vec{\vec{G}}(x, y, z \mid x', y', 0) \bullet \varepsilon \vec{M}(x', y') dx' dy' \tag{11}$$

where b and a are the aperture dimensions, and $\vec{\vec{G}}$ is the rectangular form of the dyadic, parallel-plate Green's function. The derivation of $\vec{\vec{G}}$ by Hanson and Yakovlev [7] is also represented in the polar form to provide better physical insight of the wave behavior in the parallel-plate region, namely

$$G_{t,n} = \frac{1}{(2\pi)^2} \int_0^\infty \lambda g_{t,n}(\lambda; z \mid z') \int_{-\pi}^{\pi} e^{j\lambda R\cos(\phi-\theta)} d\phi d\theta \tag{12}$$

$$g_{t,n} = \frac{\cosh p(d - |z - z'|) \pm \cosh p(d - |z + z'|)}{2p \sinh pd} \tag{13}$$

Using the complex plane analysis in [7], the polar form of the parallel-plate Green's function for (12) becomes

$$G_{t,n} = \frac{-j}{4d(1+\delta_{1,0})} H_0^{(2)}(\lambda_1 R) \bullet \left[\cos\left(\frac{l\pi}{d} \mid z - z'\right) \pm \cos\left(\frac{l\pi}{d} \mid z + z'\right) \right] \tag{14}$$

where l is the parallel-plate mode number, $\lambda_1 = \sqrt{k^2 - (l\pi/d)^2}$, and $\delta_{1,0} = 1$ for $l = 0$ and $\delta_{1,0} = 0$ for $l \neq 0$. Since having $l = 0$ is non-trivial, it is the dominant propagating mode. The 0^{th} order mode yields a propagation constant of $\lambda_0 = k = \omega\sqrt{\varepsilon\mu_0}$. The parallel-plate

Green's function exhibits a outgoing radial wave in the tranverse direction and standing wave behavior in z, which is what is expected to occur physically. Next, the Hankel function found in (14) is approximated in the far-field by

$$H_0^{(2)}(\lambda R) \sim \sqrt{\frac{2j}{\pi\lambda R}e^{-j\lambda R}} \tag{15}$$

The radial behavior of the parallel plate region in the far-field is proportional to $e^{-j\lambda R}$ [7]. The far-field wave behavior of the parallel-plate region is necessary in order to accurately characterize the edge reflection. This edge reflection occurs in the far-field of the probe and is used in the extraction of the complex permittivity.

Complex Permittivity Extraction

Upon identification of the time of the edge response as well as its amplitude using the far-field approximation in equation (15), the complex permittivity can be calculated. The following extraction method follows from Olney [12].

Based upon (14), the propagation constant inside the parallel-plate waveguide is $k = \omega\sqrt{\varepsilon\mu_0} = \beta - j\alpha$, where β is the propagation factor and α is the attenuation factor. The phase velocity for the waves can be written as

$$v_p = \frac{\omega}{\mathrm{Re}(k)} = \frac{\omega}{\beta} = v_g \tag{16}$$

where $\omega = 2\pi f$ is the angular frequency. Based upon the relations in (16) and (9), β and α are defined as

$$\beta = \mathrm{Re}(k) = \mathrm{Re}(\omega\sqrt{\varepsilon\mu_0}) = \mathrm{Re}(\omega\sqrt{\varepsilon_0\mu_0}\sqrt{\varepsilon_r}) = \mathrm{Re}(k_0\sqrt{\varepsilon_0}) = \mathrm{Re}(k_0\sqrt{\varepsilon' - j\varepsilon''}) \tag{17}$$

$$\alpha = -\mathrm{Im}(k) = -\mathrm{Im}(k_0\sqrt{\varepsilon' - j\varepsilon''}) \tag{18}$$

Since velocity is the ratio of distance over time, and the phase velocity is defined in (16), the amount of time it takes for a given electromagnetic wave to travel any given distance in the parallel-plate waveguide is defined as

$$t = \frac{d}{v_p} \tag{19}$$

The two-way travel time for a wave to propagate from an aperture to the edge and back is easily formulated

$$t_{2w} = \frac{d_{2w}}{v_p} \tag{20}$$

where d_{2w} is the distance from the center of the aperture to the edge of the flange plate and back.

In order to extract two unknowns, another relation is necessary. By knowing how the wave behaves in the parallel-plate system, the response from the edge can be modeled as

$$V_r(t) = \frac{R}{\sqrt{kd^{2w}}} e^{-\alpha d^{2w}} e^{-j\beta d^{2w}} \tag{21}$$

where R is the value representing the complex magnitude of the reflected energy from the edge. Since no measurements are done at the edge of reflection, the complex magnitude R cannot be easily determined. However if two measurements were taken with different wave travelling time, the ratio of the measurements can be used to simplify the expression. This would cancel out R and $\sqrt{k}$, which leaves α as the only unknown parameter. The equation is therefore solvable and a ratio term A is defined as

$$A = \left|\frac{V_r^{(1)}(t)}{V_r^{(2)}(t)}\right| \left(\frac{\sqrt{d_1^{2w}}}{\sqrt{d_2^{2w}}} \right) = e^{\alpha(d_2^{2w} - d_1^{2w})} \tag{22}$$

The two equations formulated thus far are required to find the complex permittivity. However, in order to compute the complex permittivity in a computationally simple method, an assumption must be made. Since $\sqrt{\varepsilon_r}$ does not have a simple closed form solution, a binomial expansion is used to approximate the relative permittivity. Through a first order expansion the relative permittivity is approximated as (since $\varepsilon'' \ll \varepsilon'$).

$$\varepsilon_r^{1/2} = (\varepsilon' - j\varepsilon'')^{1/2} = (\varepsilon')^{1/2} \left(1 - j\frac{\varepsilon''}{\varepsilon'}\right)^{1/2} \approx (\varepsilon')^{1/2} \left(1 - j\frac{\varepsilon''}{2\varepsilon'}\right) \approx \sqrt{\varepsilon'} - j\frac{\varepsilon''}{2\sqrt{\varepsilon'}} \tag{23}$$

Using the previously mentioned equations for the propagation factor and attenuation, these factors can also be approximated as follows

$$\alpha = -k_0 \operatorname{Im}(\varepsilon_r^{1/2}) \approx -k_0 \left(\frac{\varepsilon''}{2\sqrt{\varepsilon'}} \right) \approx \frac{k_0 \varepsilon''}{2\sqrt{\varepsilon'}} \tag{24}$$

$$\beta = k_0 \operatorname{Re}(\varepsilon_r^{1/2}) \approx k_0 \sqrt{\varepsilon'} \tag{25}$$

By substituting (24) and (25) into (20) and (22) an expression is formed with known values and the unknown complex permittivity parameters

$$t_{2w} = \frac{d_{2w}}{v_p} = \frac{\beta d_{2w}}{\omega} \approx \frac{k_0 \sqrt{\varepsilon'} d_{2w}}{\omega} \tag{26}$$

$$\frac{\ln(A)}{d_2^{2w} - d_1^{2w}} = \alpha \approx \frac{k_0 \varepsilon''}{2\sqrt{\varepsilon'}} \tag{27}$$

Equations (26) and (27) can be solved for the unknown values in a simple manner. The relative complex permittivity has an approximate solution for ε' given as

$$\varepsilon' \approx \left(\frac{\omega t_{2w}}{k_0 d_{2w}} \right)^2 \tag{28}$$

and ε'' is given as

$$\varepsilon'' \approx \frac{2\sqrt{\varepsilon'}\ln(A)}{k_0(d_2^{2w} - d_1^{2w})} \tag{29}$$

Dual Ridged Waveguide Behavior

The cut off frequencies of the ridged waveguide are necessary in order to determine the bandwidth available for measurement. The following is a derivation of an integral eigenvalue equation that is solved numerically by applying the Ritz-Galerkin method [5], [8].

The geometry of the dual ridged waveguide is shown in Figure 2, which is assumed to be symmetrical. The longitudinal magnetic fields in both regions must satisfy

$$(\nabla_t^2 + k_c^2) h_z(x, y) = 0 \tag{30}$$

where $k_c^2 = \gamma^2 + k^2$ is the cutoff wave number. In order to satisfy the boundary conditions, the general solution in region I becomes

$$h_z(x, y) = \sum_{n=0}^{\infty} B_{1n} \sin(k_{x1n} x) \cos\left(\frac{n\pi y}{d} \right) \tag{31}$$

where

$$\begin{aligned} k_{x1n} &= \sqrt{k_c^2 - \left(\frac{n\pi}{d} \right)^2}, \frac{n\pi}{d} < k_c \\ &= -j\sqrt{\left(\frac{n\pi}{d} \right)^2 - k_c^2}, \frac{n\pi}{d} > k_c \end{aligned} \tag{32}$$

In the same manner, the general solution in region II is

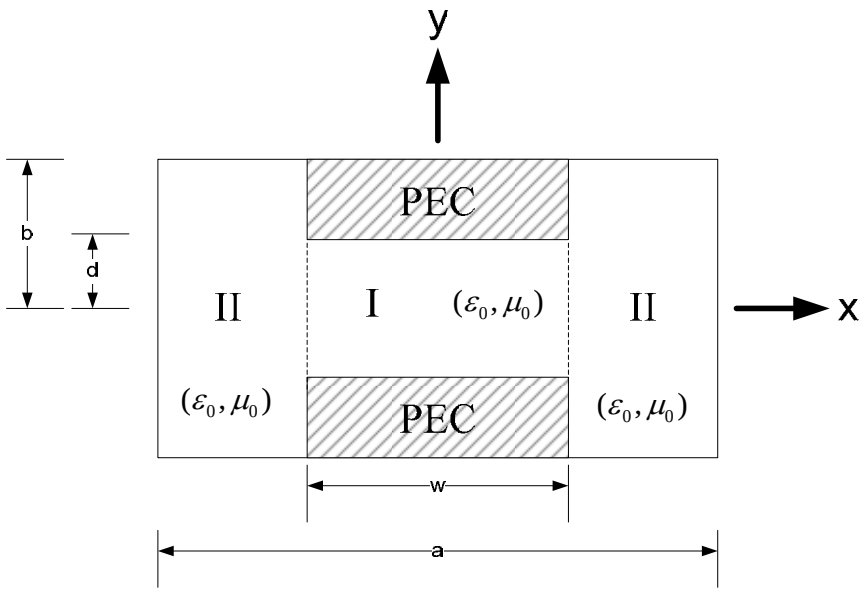

Figure 2: Geometry of dual ridged waveguide

$$h_z(x,y) = \sum_{m=0}^{\infty} B_{2m} \cos\left[k_{x2m}\left(x - \frac{a}{2}\right)\right] \cos\left(\frac{m\pi y}{b}\right) \tag{33}$$

where k_{x2m} is defined similarly to k_{x1n}. The electrical fields are given by $\vec{e}(x,y) = (j\omega\mu_0 / k_c^2)\hat{z} \times \nabla_t h_z(x,y)$. The transverse electric field in region I is

$$\begin{aligned} \vec{e}(x,y) = \frac{j\omega\mu_0}{k_c^2} \Bigg\{ & \hat{x} \sum_{n=0}^{\infty} \frac{n\pi}{d} B_{1n} \sin\left(k_{x1n} x\right) \sin\left(\frac{n\pi y}{d}\right) \\ & + \hat{y} \sum_{n=0}^{\infty} k_{x1n} B_{1n} \cos\left(k_{x1n} x\right) \cos\left(\frac{n\pi y}{d}\right) \Bigg\} \end{aligned} \tag{34}$$

and in region II is

$$\begin{aligned} \vec{e}(x,y) = \frac{j\omega\mu_0}{k_c^2} \Bigg\{ & \hat{x} \sum_{m=0}^{\infty} \frac{m\pi}{b} B_{2m} \cos\left[k_{x2m}\left(x - \frac{a}{2}\right)\right] \sin\left(\frac{m\pi y}{b}\right) \\ & - \hat{y} \sum_{m=0}^{\infty} k_{x2m} B_{2m} \sin\left[k_{x2m}\left(x - \frac{a}{2}\right)\right] \cos\left(\frac{m\pi y}{b}\right) \Bigg\} \end{aligned} \tag{35}$$

One trivial boundary condition at the junction of the two regions requires enforcement, namely the tangential electrical field at the junction must be continuous, thus

$$E(y') = \frac{j\omega\mu_0}{k_c^2}\sum_{n=0}^{\infty} k_{x1n} B_{1n} \cos\left(\frac{k_{x1n} w}{2}\right)\cos\left(\frac{n\pi y'}{d}\right)$$
$$= -\frac{j\omega\mu_0}{k_c^2}\sum_{m=0}^{\infty} k_{x2m} B_{2m} \sin\left[k_{x2m}\left(\frac{w}{2}-\frac{a}{2}\right)\right]\cos\left(\frac{m\pi y'}{b}\right) \quad (36)$$

Now an expression for the coefficients B_{1n} and B_{2m} can be written as

$$\int_0^d E(y')\cos\left(\frac{n\pi y'}{d}\right)dy' = \frac{j\omega\mu_0}{k_c^2} \in_n k_{x1n} dB_{1n} \cos\left(\frac{k_{x1n} w}{2}\right) \quad (37)$$

$$\int_0^d E(y')\cos\left(\frac{m\pi y'}{b}\right)dy' = -\left(\frac{j\omega\mu_0}{k_c}\right)^2 \in_m k_{x2m} bB_{2m} \sin\left[k_{x2m}\left(\frac{w}{2}-\frac{a}{2}\right)\right] \quad (38)$$

where $\in_0 = 1, \in_{m,n} = 1/2$ for $n \neq 0$ and $E(y') = \mathrm{e}_y(w/2, y')$ is the y component of the electric field at the junction of the two regions. The integral in (37) and (38) only has a range of $0 \le y' \le d$ since $E(y') = 0$ in $d \le y' \le b$. Substituting in the above relations into (36) and simplifying results in

$$\sum_{n=0}^{\infty} \frac{\tan\left(k_{x1n}\frac{w}{2}\right)}{\in_n k_{x1n} d}\cos\left(\frac{n\pi y}{d}\right)\int_0^d E(y')\cos\left(\frac{n\pi y'}{d}\right)dy'$$
$$= -\sum_{m=0}^{\infty} \frac{\cot\left[k_{x2m}\left(\frac{w}{2}-\frac{a}{2}\right)\right]}{\in_m k_{x2m} b}\cos\left(\frac{m\pi y}{b}\right)\int_0^d E(y')\cos\left(\frac{m\pi y'}{b}\right)dy' \quad (39)$$

Equation (39) can be written as a integral eigenvalue equation of $\bar{L}(k_c) \bullet E(y') = 0$. The solution to the eigenvalue problem is very complicated since $\bar{L}(k_c)$ involves a complex integral-summation operator. However, a numerical solution is possible by applying the Ritz-Galerkin method. This method expands the unknown boundary electrical field by a truncated set of suitable functions, namely

$$E(y') = \sum_{p=0}^{P} C_p \cos\left(\frac{p\pi y'}{d}\right) \tag{40}$$

Then (40) is substituted into (39), multiplied by $\cos(q\pi y / d)$, and the summation on m is truncated to M, which yields a matrix equation of the form

$$[A(k_c)][C] = 0 \tag{41}$$

with matrix elements given by

$$A_{ij} = \delta_{ij} \frac{\tan\left(k_{x1i}\frac{w}{2}\right)}{k_{x1i}} \in_i d + \sum_{m=0}^{M} \frac{\cot\left[k_{x2m}\left(\frac{w}{2}-\frac{a}{2}\right)\right]}{\in_m k_{x2m} b} I_{im} I_{jm} \tag{42}$$

where

$$I_{rm} = \int_0^d \cos\frac{r\pi y}{d} \cos\frac{m\pi y}{b} dy \tag{43}$$

and δ_{ij} is the Kronecker delta. Equation (41) is a generalized eigenvalue problem where the eigenvalues k_c are the solutions of the nonlinear equation

$$\det\left|A(k_c)\right| = 0 \tag{44}$$

Given the dimensions of a dual ridged waveguide, the eigenvalues or mode frequencies can be numerically found as well as the usable bandwidth. Therefore, measurements can be taken using the dominant mode of the dual ridged waveguide.

Summary

This chapter gave a brief review of the principles in EM theory needed to perform the analysis and associated experiments in this thesis. First, the parameters for complex permittivity were defined so that they can be analytically extracted. Then, the behavior

of EM waves in the far-field of the parallel-plate waveguide was described, as well as, a simple parameter extraction technique that is used to approximate the complex permittivity. Lastly, the wave behavior in a dual ridged waveguide is derived in order to determine the main propagating mode frequency and bandwidth.

III. Methodology

The method for extracting the complex permittivity from simple media is detailed. First the measurement system setup and calibration is described. Next, the frequency range available for the measurements is determined. Finally, the data processing techniques from the raw time domain data are described in order to extract the complex permittivity of the dielectric material.

Measurement System

The measurement system consists of several components that are shown in Figure 3. The system is made up of a NWA, connector cables, WRD650 dual ridged waveguide and assorted size and shape flange plates.

All of the flange plates have an aperture that matches the one found for the dual ridged waveguide so that all of the EM fields are able to propagate unimpeded. Also, each flange plate has the appropriate pin and screw holes so that the apertures align properly when attached to the waveguide. The flange plates have two different geometries and have various dimensions. The circular flange plates are 6 inches and 4 inches in diameter. The square flange plates are 6 inches, 4 inches and 1.5 inches.

The measurement system is assembled by attaching a flange plate directly onto the waveguide with the apertures lined up. The waveguide is attached to an adapter for the cables, which then lead to the NWA. Figure 4 shows an example of the waveguide probe.

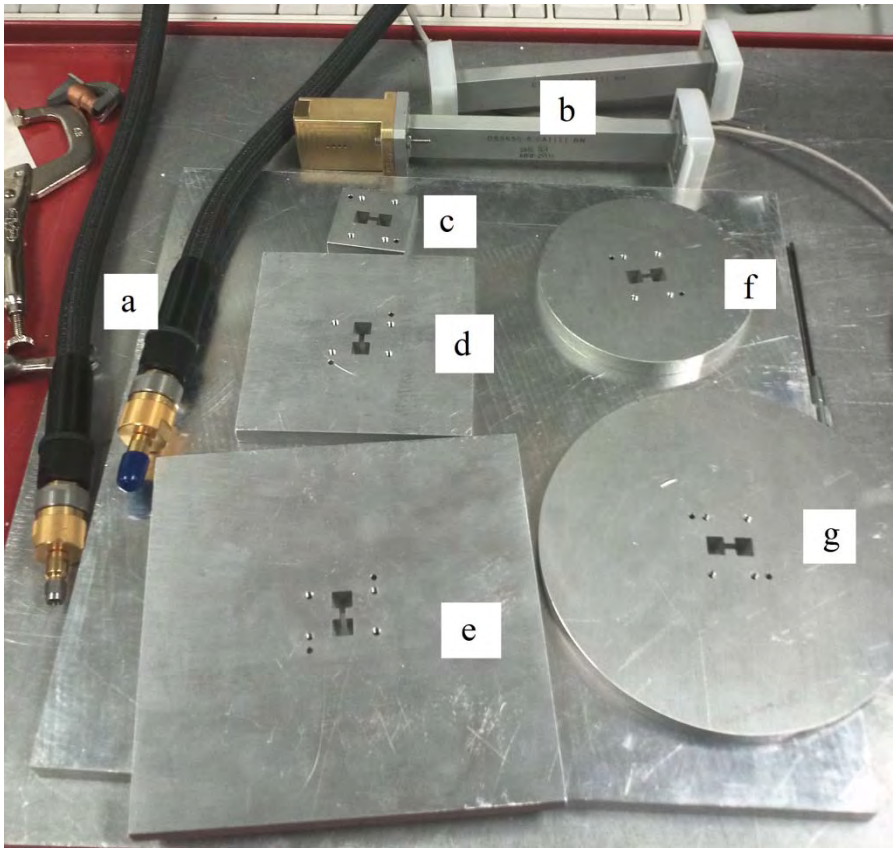

Figure 3: Measurement system components: (a) cables leading to NWA, (b) WRD650 dual ridged waveguide, (c) 1.5" square plate, (d) 4" square plate, (e) 6" square plate, (f) 4" diameter circular plate, (g) 6" diameter circular plate

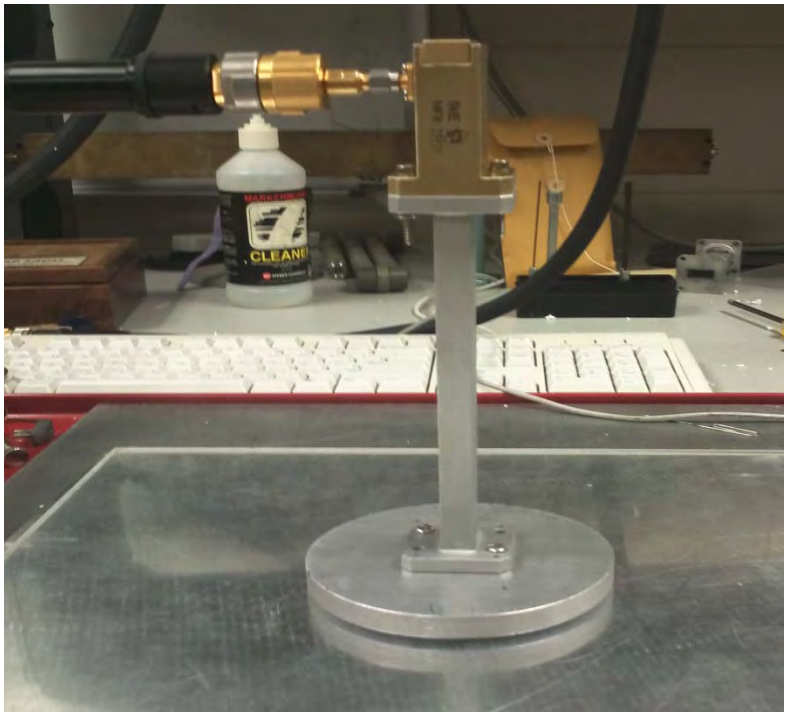

Figure 4: Waveguide measurement probe with 4" circular flange plate

Calibration

The calibration of the waveguide probe is accomplished by using a 3 short method. The advantages of this method are that this one port calibration will remove the system errors from the S_{11} measurement. This calibration will allow the reference plane to be set at the end of the flange plate, which is where the aperture meets the sample dielectric material. Any given measurement on the NWA has errors that can be corrected by solving for the system S-parameters.

$$S_{11}^{ms} = S_{11}^{A} + \frac{S_{21}^{A} S_{12}^{A} S_{11}^{1}}{1 - S_{22}^{A} S_{11}^{1}} \tag{45}$$

where $S_{11}^{A}, S_{21}^{A} S_{12}^{A}, S_{22}^{A}$ are the unknown system S-parameters, S_{11}^{ms} is the measured reflection, and S_{11}^{1} is the calculated reflection. The use of three distinct shorts allows the above equations to be formulated for the unknown parameters. A short at any given length has a reflection as

$$S_{11}^{sh} = -1e^{-jk_z(l)} \tag{46}$$

where $k_z = \sqrt{k_0^2 - k_c^2}$ and l is the two-way length of the offset from the reference plane. The manufacturer gives the waveguide a cutoff frequency of 5.567 GHz. With 3 distinct short measurements and their calculated reflections, a system of 3 equations can be solved for the system S-parameters

$$S_{22}^{A} = \frac{S_{11}^{sh1}(S_{11}^{m2} - S_{11}^{m3}) + S_{11}^{sh2}(S_{11}^{m3} - S_{11}^{m1}) + S_{11}^{sh3}(S_{11}^{m1} - S_{11}^{m2})}{S_{11}^{sh1} S_{11}^{sh2}(S_{11}^{m2} - S_{11}^{m1}) + S_{11}^{sh1} S_{11}^{sh3}(S_{11}^{m1} - S_{11}^{m3}) + S_{11}^{sh2} S_{11}^{sh3}(S_{11}^{m3} - S_{11}^{m2})} \tag{47}$$

$$S_{21}^{A} S_{12}^{A} = \frac{(S_{11}^{m1} - S_{11}^{m2})(1 - S_{22}^{A} S_{11}^{sh1})(1 - S_{22}^{A} S_{11}^{sh2})}{\left[S_{11}^{sh1}(1 - S_{22}^{A} S_{11}^{sh2}) - S_{11}^{sh2}(1 - S_{22}^{A} S_{11}^{sh1}) \right]} \tag{48}$$

$$S_{11}^{A} = S_{22}^{m1} - \frac{S_{21}^{A} S_{12}^{A} S_{11}^{sh1}}{1 - S_{22}^{A} S_{11}^{sh1}} \tag{49}$$

where $S_{11}^{m1}, S_{11}^{m2}, S_{11}^{m3}$ are the measured reflections for each short and $S_{11}^{sh1}, S_{11}^{sh2}, S_{11}^{sh3}$ are the calculated reflections for each short. In order to have the reference plane at the end of the flange, the first short is measured with the flange attached to the waveguide, which gives it a length of 0. The second short is measured with a 6.96 mm thru piece attached. The third short is with nothing attached to a waveguide, giving it an offset equal to the flange width, which is 9.77 mm. Since the reference plane is with flanges attached, all of the other short lengths are considered negative distances. Figure 5 shows the configuration of the 3 distinct shorts. In order to minimize flange plate reattachment, the calibration is done by measuring short 1 last. Knowing the system S-parameters, any reflection

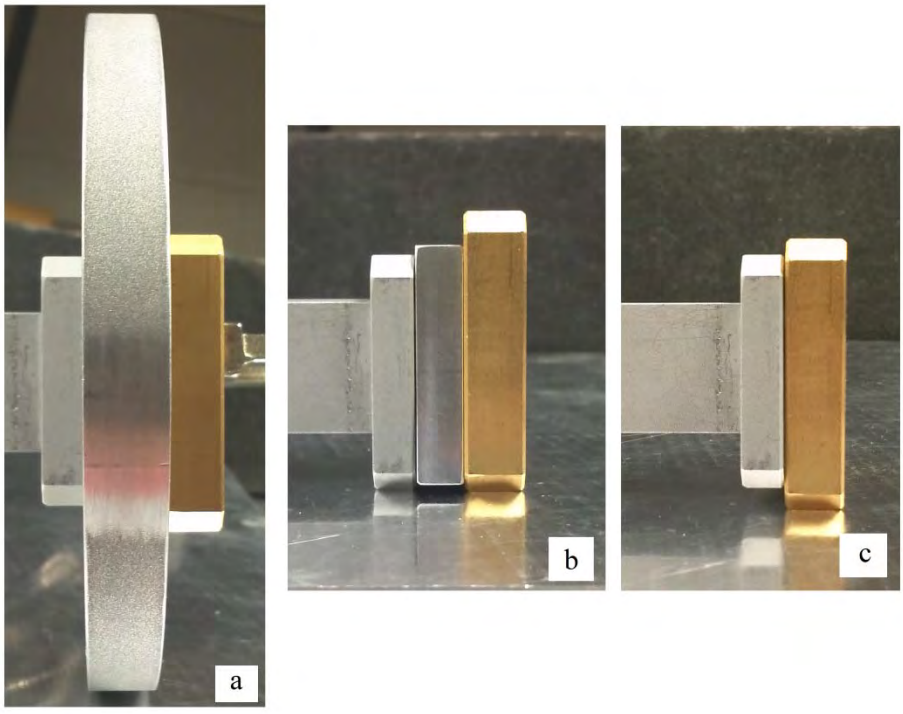

Figure 5: Short measurement setup: (a) Short 1, (b) Short 2, (c) Short 3

measurement can be processed to remove the system errors. By rearranging (45), calibrated measurements are calculated by

$$S_{11} = \frac{S_{11}^{ms} - S_{11}^{A}}{S_{21}^{A} S_{12}^{A} + S_{22}^{A} S_{11}^{ms} - S_{11}^{A} S_{11}^{A}} \tag{50}$$

However, one limitation exists in the 3 short method. The largest reference plane distance must be approximately half of the z-directed wavelength, which is given by

$$\lambda_z = \frac{c}{f\sqrt{1-\left(\frac{f_c}{f}\right)^2}} \tag{51}$$

where f is the highest frequency used. Thus, $\lambda_z / 2$ needs to be greater than 9.77 mm, which is the flange plate thickness. By using a high frequency of 15 GHz, $\lambda_z / 2$ = 10.76 mm. Thus, a high frequency of 15 GHz is acceptable to use, since the flange plates are thinner than $\lambda_z / 2$.

Frequency Range

Although the thickness dimension of the flange plates limits the upper frequency range during calibration, the frequency range of the dual ridged waveguide needs to be discussed. The frequency range is found by finding the cutoff frequencies of the two lowest modes by solving (44) with matrix elements given by (42). The physical dimensions of the waveguide are as follows: w=0.173", a=0.720", d=0.0505" and b=0.1605". The nonlinear eigenvalue problem can be solved by the Secant method

$$x_n = x_{n-1} - f(x_{n-1}) \frac{x_{n-1} - x_{n-2}}{f(x_{n-1}) - f(x_{n-2})} \tag{52}$$

Based on two initial guesses, which should be close to the root, the recurrence relation will converge on a root. The nonlinear solution to k_c behaves very asymptotic as shown in Figure 6. Using the dimensions of the waveguide and the secant method, the first two modes of the waveguide are calculated to be 5.567 GHz and 22.728 GHz, respectively. However, a common rule of thumb is to operate approximately 25% above the low end cutoff and 5% below the high end cutoff. This is to ensure that the waves behave appropriately and so that other modes are not excited. This changes the usable bandwidth of the dual ridged waveguide to 6.5 GHz to 18 GHz.

Another factor that may limit the bandwidth of the measurement probe is the frequency range of the parallel-plate waveguide. The parallel-plate region is created by

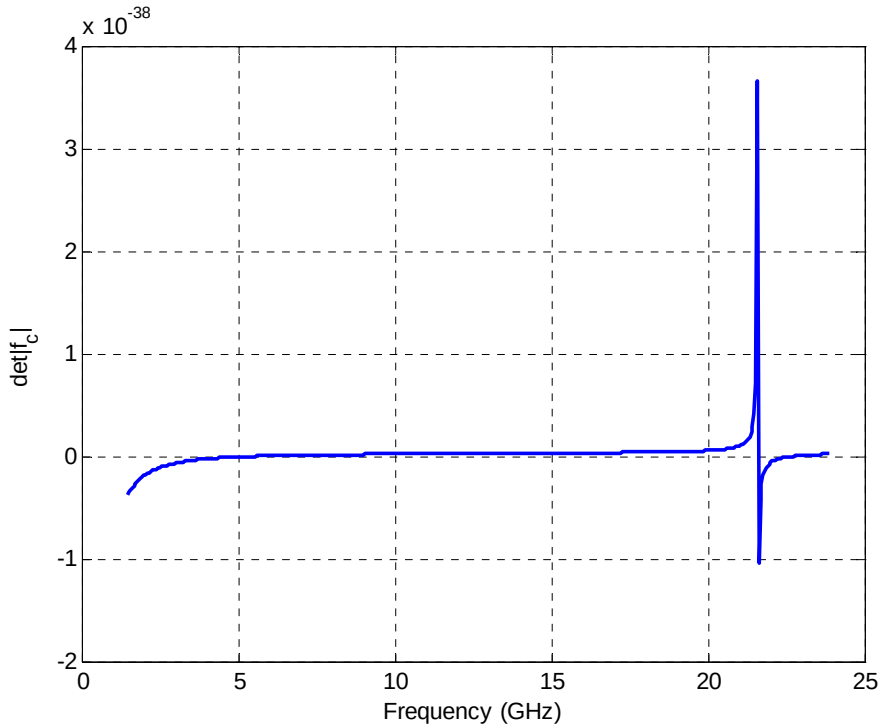

Figure 6: $\det|k_c|$ **of WRD650 Waveguide.**

the PEC backed dielectric sample and the flange plate on the waveguide probe. The cutoff frequency for a parallel-plate waveguide is

$$f_c = \frac{c}{2\sqrt{\varepsilon_r}}\left(\frac{n}{a}\right) \tag{53}$$

where n is the mode number and a is the distance between the parallel plates [3]. As discussed in Chapter 2, the 0^{th} order mode is a non-trivial solution which gives an $f_c = 0$ GHz. However, the 1^{st} mode depends on the complex permittivity and the plate separation. Since the method to extract the complex permittivity relies on the wave behavior to have single mode operation, the upper limit of the frequency of the parallel-plate waveguide is important. Since the complex permittivity is necessary to solve for the cutoff frequency in (53), this becomes an issue considering that is the parameter in question. One method to observe whether higher order modes are being excited is to observe the $S_{11}(\omega)$ measurement and heuristically determine if those modes are excited. An example of the $S_{11}(\omega)$ response is shown in Figure 7, however, no heavy oscillation is observed at the higher frequencies. One may also analytically compute the cutoff of the first higher-order parallel plate mode via (53) assuming ϵ_r is known.

Given the various frequency constraints of the dual ridged waveguide, parallel-plate waveguide, and calibration, the frequency range of the system is 6.5 GHz to 15 GHz. The lower limit is dependent on the cutoff frequency of the WRD650 waveguide and the upper limit is a result of the calibration method and availability of standards. However, the thickness and type of material used may excite higher modes, which means that either the method needs to be changed or the upper limit frequency requires truncation.

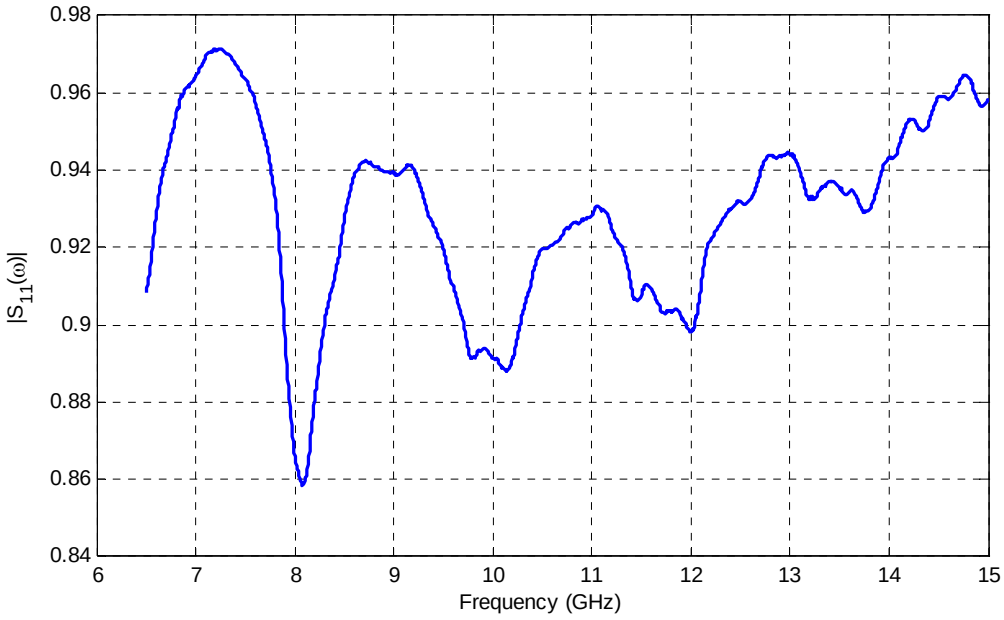

Figure 7: Frequency Domain Data from waveguide probe with no 1st order mode excitation in the parallel-plate region

Data Processing

Once the system is calibrated, measurements can be taken with an unknown dielectric sample. The measurement occurs by placing the PEC-backed dielectric sample under the waveguide probe as shown in Figure 4. The NWA performs stepped frequency measurements, which are subsequently transformed into the time-domain using an inverse Fourier transform. An example of transformed S_{11} data is shown in Figure 8. Although there is a large main reflection, it is sometimes difficult to distinguish the side

lobes, which show the flange plate reflection. Therefore, additional signal processing is required to observe a more dominant edge reflection.

Fourier Transform

The frequency-domain data collected needs to be processed into the time-domain. A common method is to use Fourier transforms. Since the NWA data is a discrete sampling, transforms are performed using the discrete Fourier Transform (DFT). The DFT pair is given as

$$x(n) = \frac{1}{N}\sum_{k=0}^{N-1} X[k] e^{j\frac{2\pi}{N}kn} \tag{54}$$

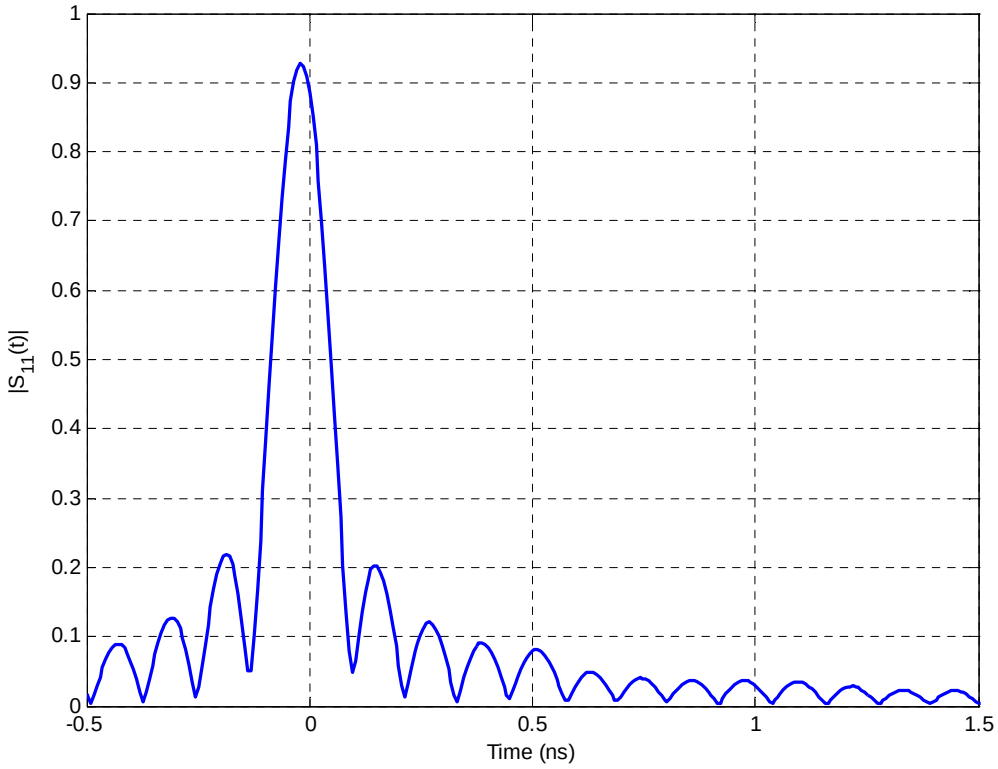

Figure 8: Time domain data of a 4" diameter circular plate

$$X[k] = \sum_{n=0}^{N-1} x(n) e^{-j\frac{2\pi}{N}kn} \tag{55}$$

where N is the number of samples for the frequency, $X[k]$, and time domain, $x(t)$, data. One important artifact arises out of the use of the DFT. Since the DFT is periodic, it is important to understand the effects that a finite spectral bandwidth (BW) and the frequency step size (df) have on the temporal resolution (T_s), which in turn effects the alias-free time span (T_{AF}). The temporal resolution, T_s, can be approximated using the frequency step size as

$$T_s = \frac{1}{Ndf} = \frac{1}{BW} \tag{56}$$

Using this information, the alias-free range for the time-domain data can be determined by $T_{AF} = NT_s$ [10].

Windowing

Based on the raw time domain data shown in Figure 8, it is hard to determine the edge reflection from the measurements. Additional signal processing in the form of windowing is necessary. Windowing will allow the edge reflection to be isolated in the signal allowing for the extraction of the complex permittivity. Two windows have been chosen for the signal processing. The Kaiser and Blackman-Harris windows perform best in detection of nearby tones of significantly different amplitudes [4].

The Kaiser window is given by

$$w(t) = \begin{cases} \dfrac{I_o\left[\beta\sqrt{1-(2t)^2}\right]}{I_0(\beta)}, 0 \le |t| \le \dfrac{1}{2} \\ 0 \qquad\qquad , else \end{cases} \tag{57}$$

in the time domain and

$$W(f) = \frac{\sin\left(\sqrt{\pi^2 f^2 - \beta^2}\right)}{I_0(\beta)\sqrt{\pi^2 f^2 - \beta^2}} \tag{58}$$

in the frequency domain. I_0 is the zeroth order modified Bessel function of the first kind. The value β is a Kaiser window parameter that affects the sidelobe attenuation and main lobe width of the Fourier Transform of the window.

One important note is the fact that β can be adjusted in order to suppress the main response so that the smaller amplitude responses become more visible. Figure 9 shows a comparison of the Kaiser window with a small β value. Figure 10 shows temporal data with various β values. It can be seen that a small value of β does not

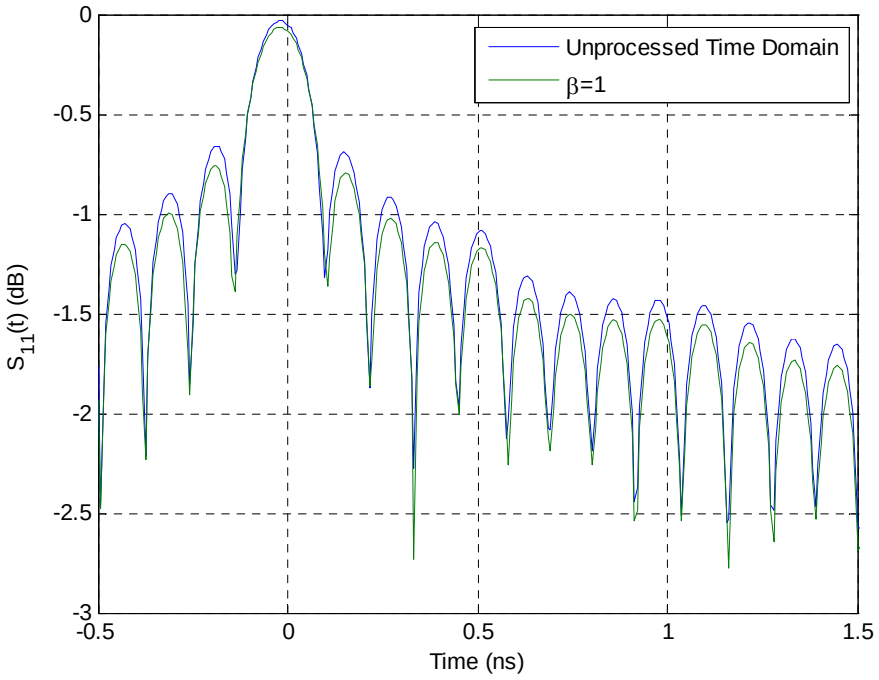

Figure 9: Time-domain data showing unprocessed data and Kaiser windowing with $\beta = 1$

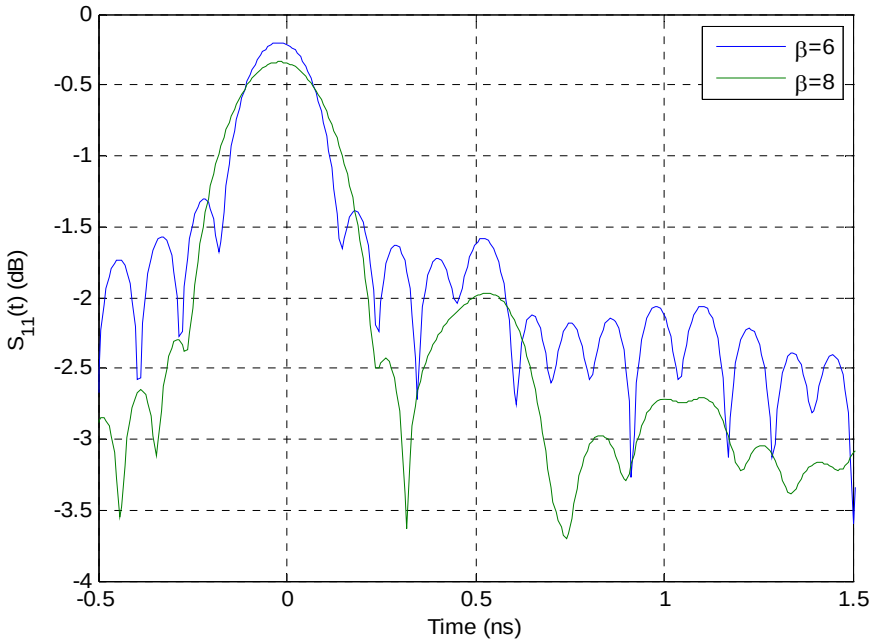

Figure 10: Kaiser windowing with respective β values

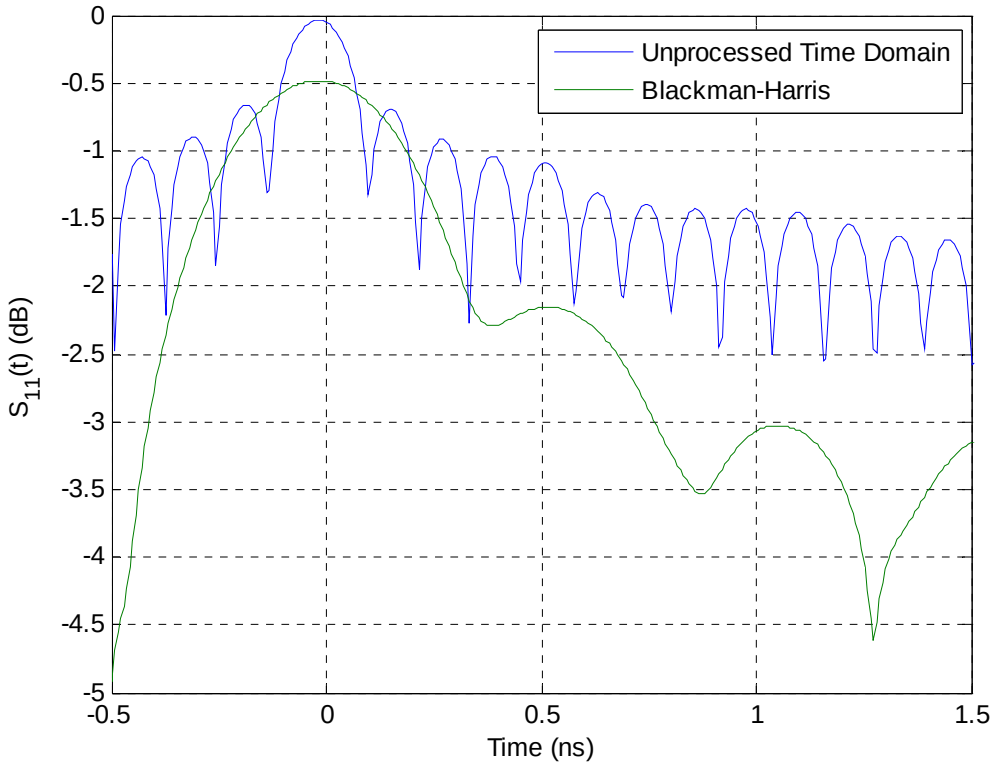

Figure 11: Time-data showing the unprocessed signal and Blackman-Harris windowing

show a prominent edge response, however, a larger β clearly reveals the edge reflection considerably.

The Blackman-Harris window is given by

$$w(t) = a_0 - a_1 \cos\left(\frac{2\pi t}{N-1}\right) + a_2 \cos\left(\frac{4\pi t}{N-1}\right) - a_3 \cos\left(\frac{6\pi t}{N-1}\right) \tag{59}$$

in the time domain, where $a_0 \approx 0.3636$, $a_1 \approx 0.4892$, $a_2 \approx 0.1366$, $a_3 \approx 0.0106$, and N is the number of points in the window. The Blackman-Harris window trades main lobe width for a higher sidelobe level, which makes it suitable for signal detection. An example of the Blackman-Harris window is compared with a unprocessed time-domain signal in Figure 11.

Summary

In this chapter, the setup and calibration of the dual ridged waveguide probe is discussed. The frequency range available for measurement has been calculated to avoid the propagation of higher order modes as well as to make the calibration valid. A method is described to avoid exciting higher order modes in the parallel-plate waveguide. Measurements in the next chapter take into account all of the precautions described in this chapter. Two different signal processing windows have been described to be used to detect the edge reflection, which can then be extracted using an approximation described in Chapter 2. The experiment will try to show that the use of a dual ridged waveguide coupled into a parallel-plate waveguide will produce a distinguishable edge reflection which is processed to extract the complex permittivity. The results from applying this method will be shown in Chapter 4.

IV. Analysis and Results

The method in Chapter 3 is applied and the results are presented in this chapter. The measurements are performed using two different Plexiglas samples as the dielectric. In order to know how accurate the final extraction is, the uncertainty associated with the measurement process is analyzed so that confidence intervals can be created for the final complex permittivity extraction. The two windowing signal processing methods are presented to show the edge response. These results are then used to extract the permittivity with the associated confidence intervals.

Sources of Error

Any experiment has some sort of error involved. By being able to identify the points at which error occur, the accuracy and effectiveness of the method can be assessed.

The sources of error must be first indentified before any uncertainty can be calculated for the complex permittivity. The first error terms deal with the variables involved in (15) and (16). These equations provide four different variables, which are measured. The first variable is the distance from the center of the aperture to the edge of the flange plate and back. No matter how precisely machined, the square or circular flange plates will never be ideal. The two way distance, d_{2w}, is measured by a digital caliper. The rest of the variables are: angular frequency, ω; two way time, t_{2w}; and the ratio of the complex response amplitudes, A. These values are measured by the NWA, and two of the values (t_{2w} and A) are calculated through the described signal processing methods.

The NWA averages values and uses an IF bandwidth to reduce the noise level in the measurements. The value A is a ratio, and the signal processing involved will apply similar mathematical errors on the signal. The uncertainty on A is assumed to be negligible.

Temporal and Spectral Variables

The NWA manual [2] states that the minimum frequency domain resolution is 1 Hz. Given this resolution as the worst case scenario for a frequency measurement, the frequency step size is orders of magnitude greater than this uncertainty. Therefore, the NWA resolution is considered to be negligible.

The temporal domain uncertainty has two factors. The first is proportional to the uncertainty of the frequency measurements. However, since the frequency uncertainty is considered to be negligible, the time domain uncertainty is negligible with respect to the frequency measurement. The second time domain uncertainty factor arises from the Fourier analysis. Equation (56) relates the time domain resolution to the bandwidth of the frequency measurements taken. This leaves an uncertainty whether the edge response is within an irresolvable region of the IFT. There is an assumption that the edge reflection peak occurs at a location closer to the point identified as the edge reflection than any other point. The actual edge reflection, x, must lie in the area of $-T_s / 2 \le x \le T_s / 2$. This time range is centered on the point that is identified as the edge response. The actual edge reflection is not dependent on the Fourier analysis. Therefore, it is possible that the edge response can occur anywhere within the area with an equal probability. This gives a probability density (i.e. uniform distribution) of the time of the edge reflection to be

defined as a unit step function [1]. The standard uncertainty, u, for the time of the occurrence of the edge reflection is therefore

$$u = \frac{T_s}{2\sqrt{3}} \tag{60}$$

Distance Variable

The dimensions of the square and circular flange plates were measured with a precision digital caliper. The two way distance traveled by the EM wave can be calculated using these measurements. Each flange plate was measured 20 times in various locations of the plate in order to form a statistical analysis. The flange plates exhibited a Guassian (normal) PDF with a low standard deviation. The distributions of the plate measurements along with a Guassian curve are shown in Figure 12. Table 1 shows the mean and standard deviation. This is necessary to form the basis of the uncertainty associated with the distance in the extraction method.

Table 1: Statistical Data from 20 measurements of each plate used in measurements

	Mean (mm)	Standard Deviation (mm)
6” Square Plate	152.45	0.0163
4” Square Plate	101.62	0.0190
1.5” Square Plate	38.12	0.0144
6” Circular Plate	152.43	0.0136
4” Circular Plate	101.62	0.0081

Overall Uncertainty

The two largest uncertainties are the physical measurements of the distance traveled by the wave in the parallel-plate system and the time variable resolution. These uncertainties must be taken into account, since they may represent a large error in the

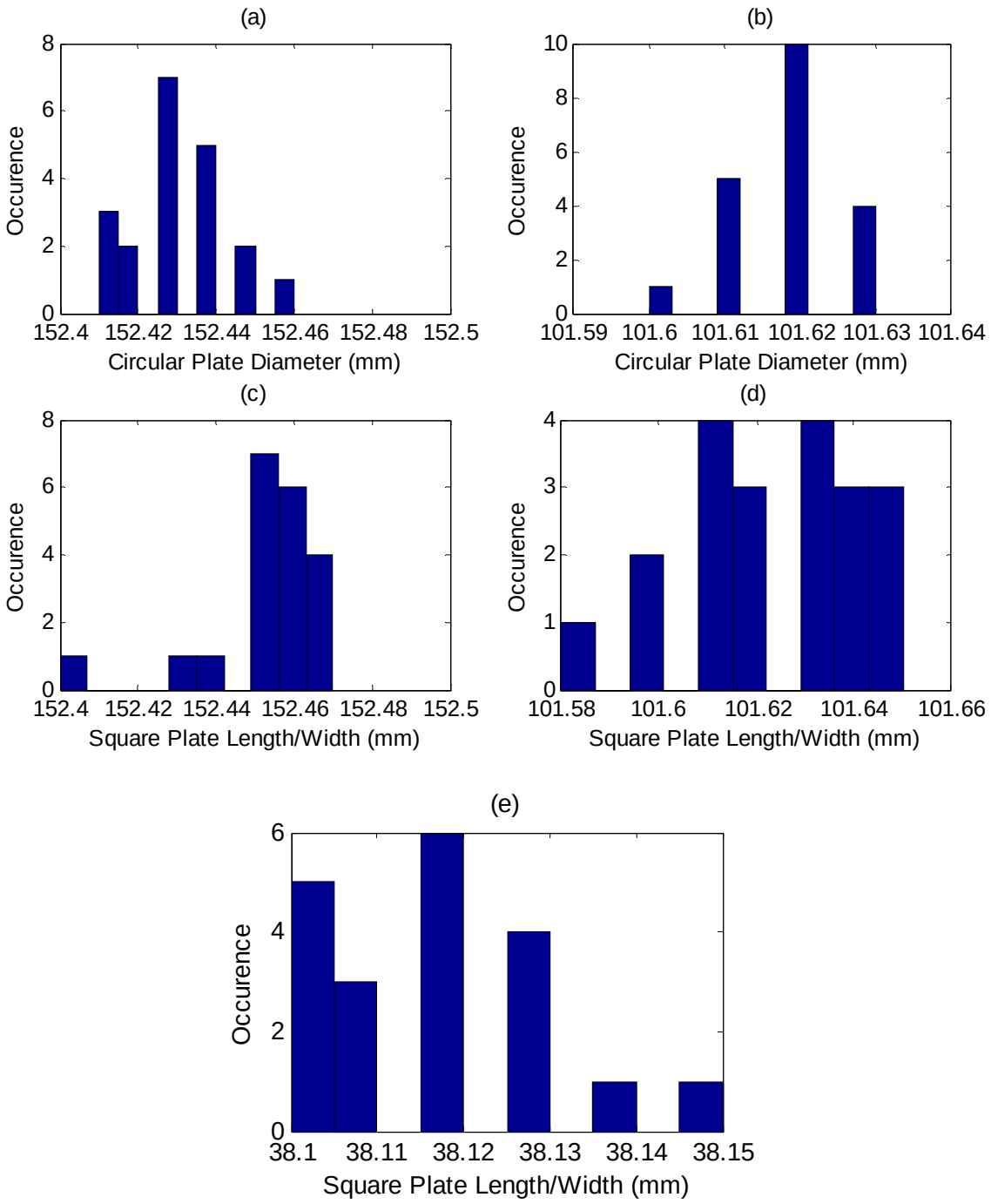

Figure 12: Histograms for the dimensions of (a) 6" Circular Plate, (b) 4 Circular Plate, (c) 6" Length/Width Square Plate, (d) 4" Length/Width Square Plate, and (e) 1.5" Length/Width Square Plate

complex permittivity extraction. The real part of the relative complex permittivity can be computed by [11]

$$\delta\varepsilon'(d,t) = \frac{\partial\varepsilon'(d_0,t_0)}{\partial d}\delta d + \frac{\partial\varepsilon'(d_0,t_0)}{\partial t}\delta t \tag{61}$$

where d and t are the distance and time variables, the subscript zero is the expected values and δ is the uncertainty. The imaginary part of the relative complex permittivity can be written as

$$\begin{aligned}\delta\varepsilon''(d_1,d_2,\varepsilon') = {} & \frac{\partial\varepsilon''(d_{1_0},d_{2_0},\varepsilon_0')}{\partial d_1}\delta d_1 + \frac{\partial\varepsilon''(d_{1_0},d_{2_0},\varepsilon_0')}{\partial d_2}\delta d_2 \\ & + \frac{\partial\varepsilon''(d_{1_0},d_{2_0},\varepsilon_0')}{\partial\varepsilon'}\delta\varepsilon'\end{aligned} \tag{62}$$

where d_{1_0} and d_{2_0} are the expected values for d_1 and d_2 and ε_0' is the expected value for ε'.

Data Processing Results

The first step in the data processing is to perform an IFFT and then window the data with one of the methods described in Chapter 3. After that, this information can be used to perform the complex permittivity extraction. Both of the processing windows try to resolve an edge response, however, the extent of the accuracy and effectiveness of the windows cannot be known until the final extraction. In order to have a gauge on the effectiveness of a signal processing method, the ideal response time will be annotated. The industry value standard for the real part of the relative complex permittivity is 2.6 and is used to calculate the theoretical edge response time.

Kaiser Windowing

The Kaiser window is able to suppress the inherent signal processing sidelobes in order that lower level signal responses become more apparent. Since the signal is processed, the information collected may be altered more than expected. The sample dielectric material used in the measurements is 4.39 mm thick and 5.55 mm thick Plexiglas. Based on the frequency range conclusions in Chapter 3, the frequency range used for all measurements is 6.5 GHz to 15 GHz. Figures 13-22 show the time domain signal, Kaiser windowed time domain signal and the ideal edge reflection time. The Kaiser window is applied with a β value of 8 for the 4" and 6" circular and square flange plates. Since 1.5" will yield a response much closer to the main lobe, a smaller β value of 4 is used to be able to bring out the edge response. The data measurements were taken using 6" circular, 4" circular, 6" square, and 4" square, and 1.5" square flange plates. The unprocessed time signal is shown with the Kaiser window to show that difference the signal processing can have on the transformed data.

As shown from the time domain figures, it is very difficult to determine the edge reflection without any further signal processing. Table 2 compares the measured reflection times with the ideal reflections times of 0.82 ns, 0.55 ns, and 0.21 ns for the 6", 4", 1.5" flanges plates, respectively. The Kaiser windowing is able to show an edge response to a close degree of accuracy.

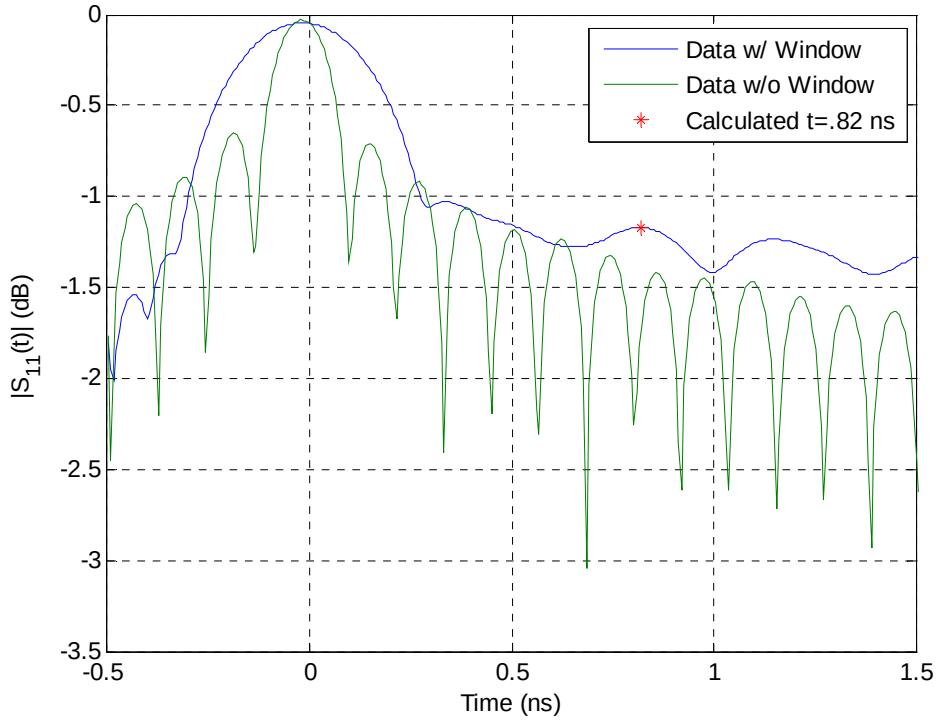

Figure 13: Time Data with Kaiser window from 6" Square plate with 5.55mm thick Plexiglas sample

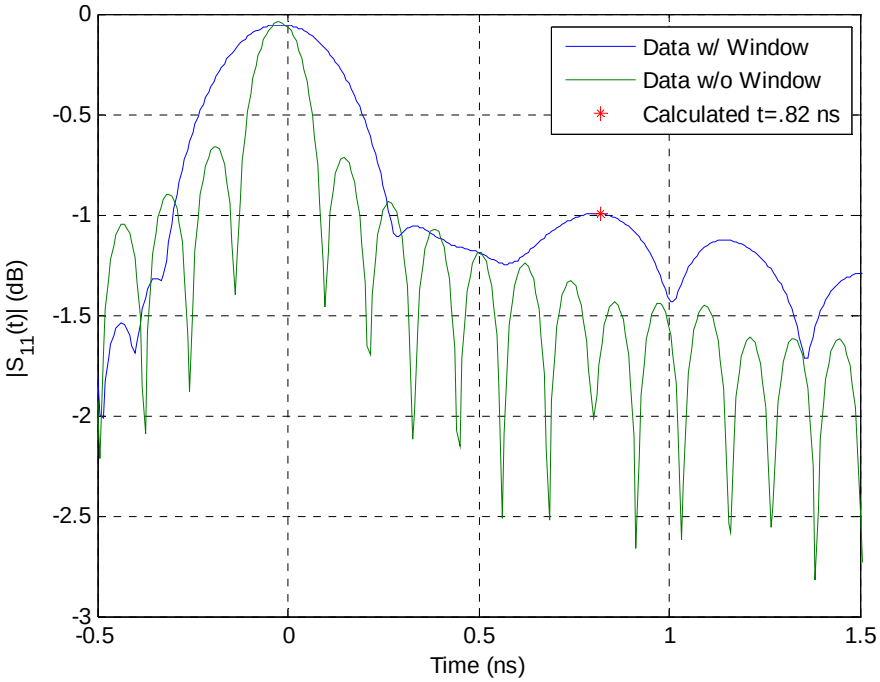

Figure 14: Time Data with Kaiser window from 6" Square plate with 4.39mm thick Plexiglas sample

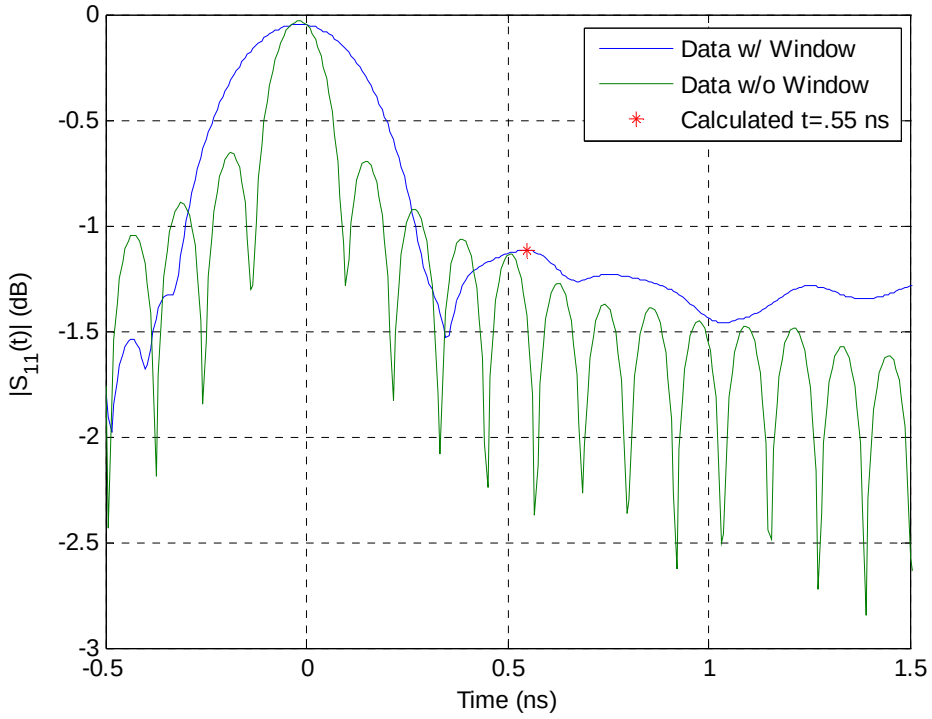

Figure 15: Time Data with Kaiser window from 4" Square plate with 5.55mm thick Plexiglas sample

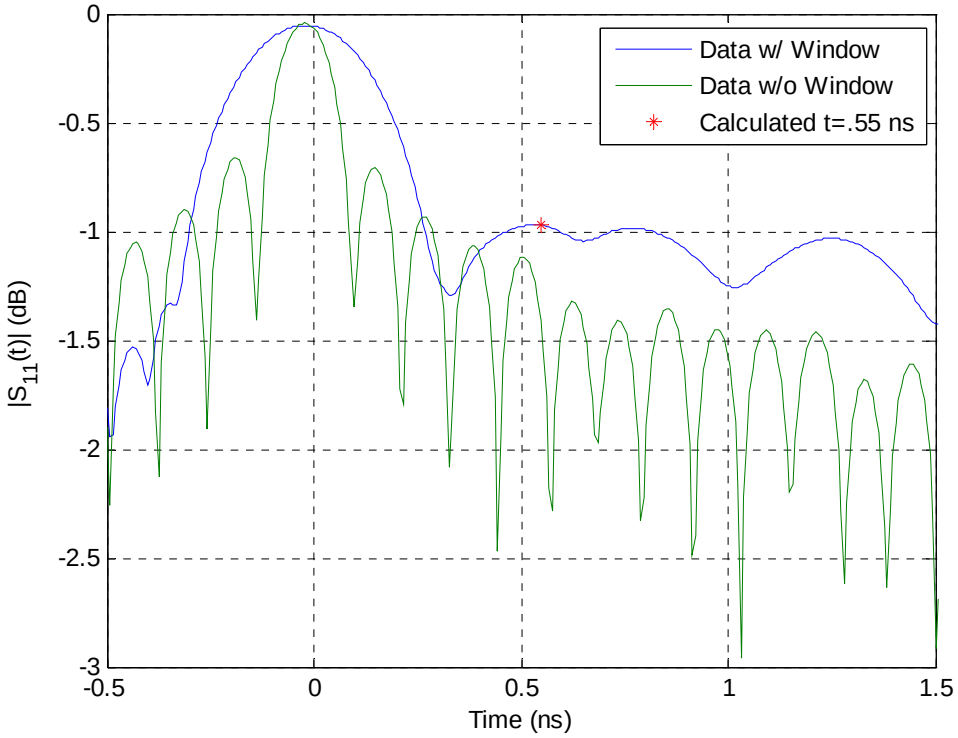

Figure 16: Time Data with Kaiser window from 4" Square plate with 4.39mm thick Plexiglas sample

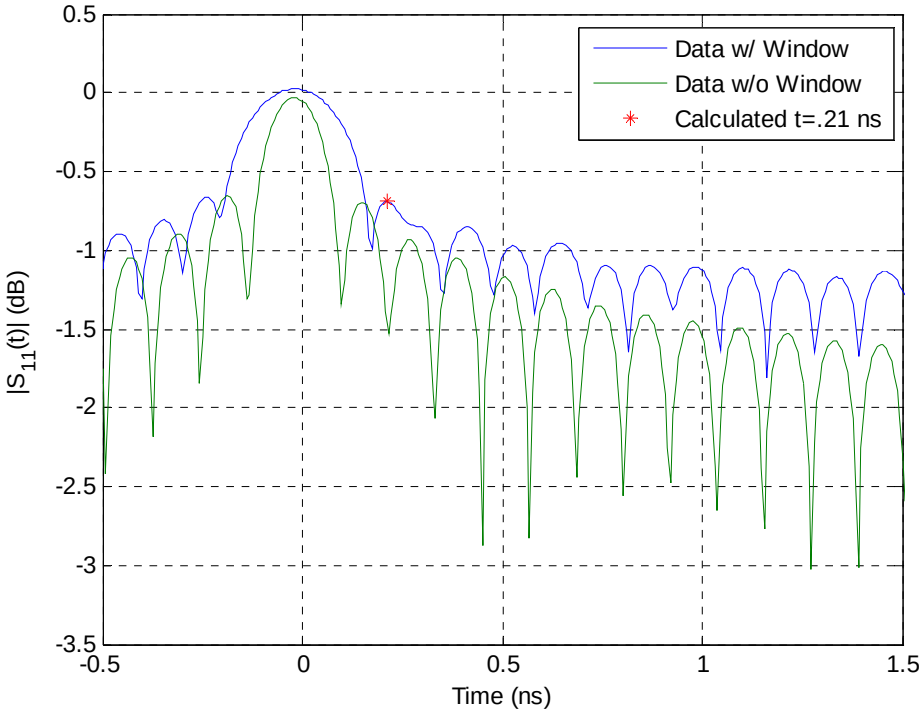

Figure 17: Time Data with Kaiser window from 1.5" Square plate with 5.55mm thick Plexiglas sample

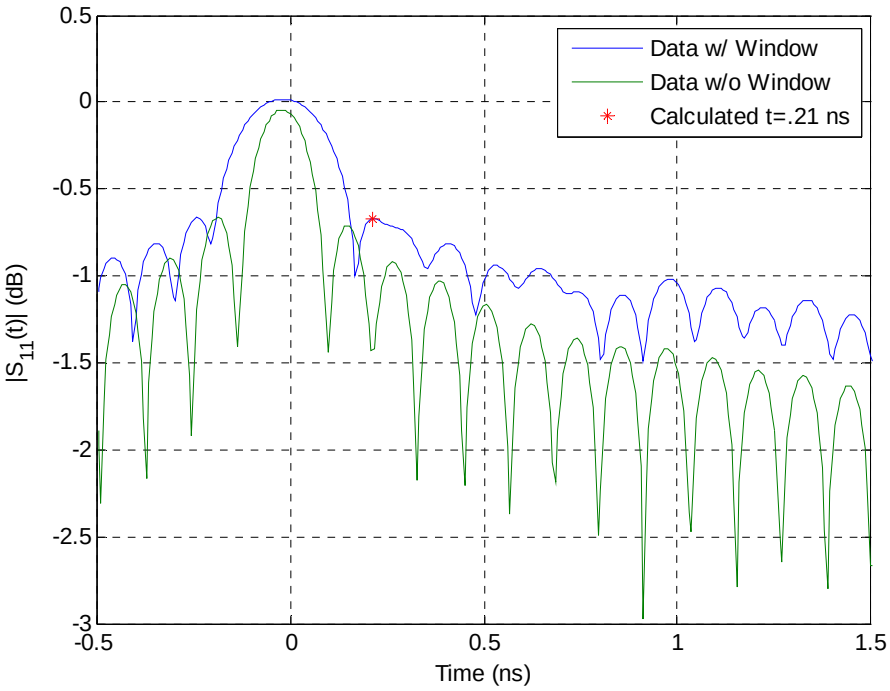

Figure 18: Time Data with Kaiser window from 1.5" Square plate with 4.39mm thick Plexiglas sample

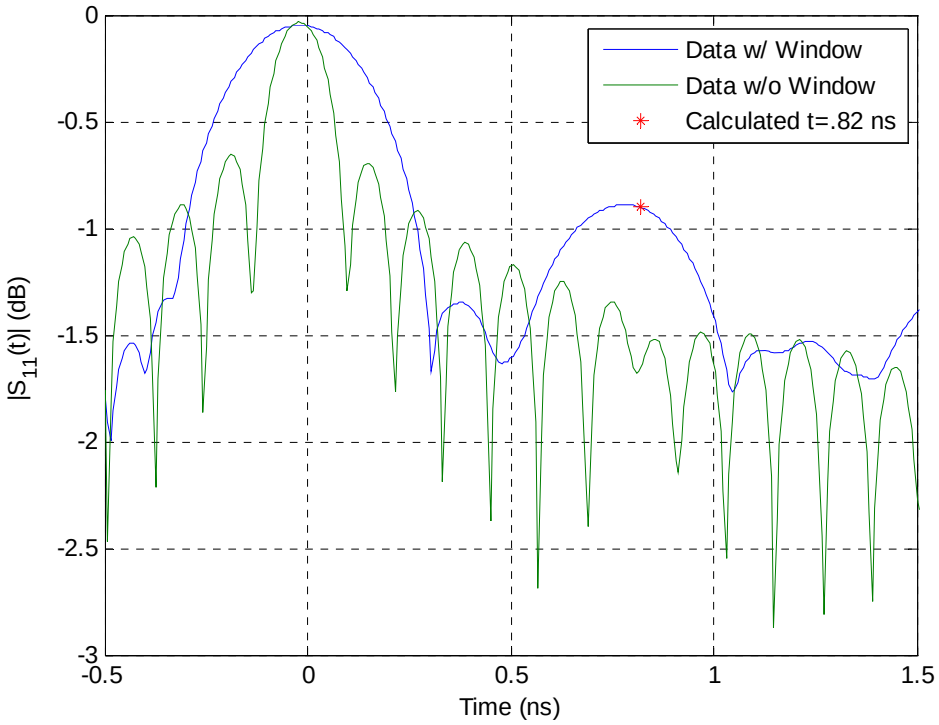

Figure 19: Time Data with Kaiser window from 6" Circular plate with 5.55mm thick Plexiglas sample

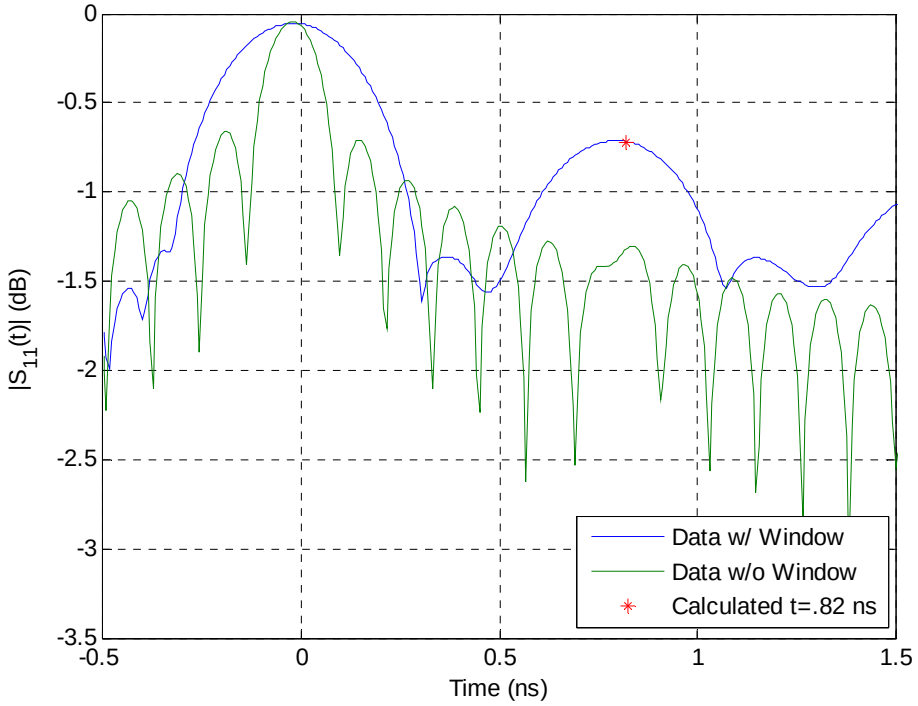

Figure 20: Time Data with Kaiser window from 6" Circular plate with 4.39mm thick Plexiglas sample

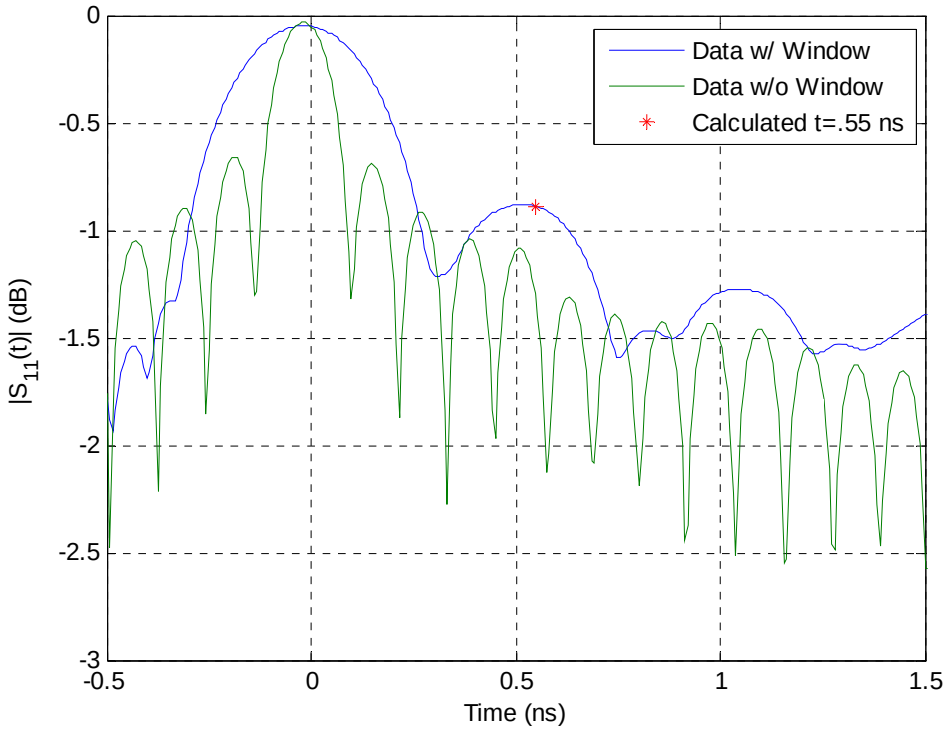

Figure 21: Time Data with Kaiser window from 4" Circular plate with 5.55mm thick Plexiglas sample

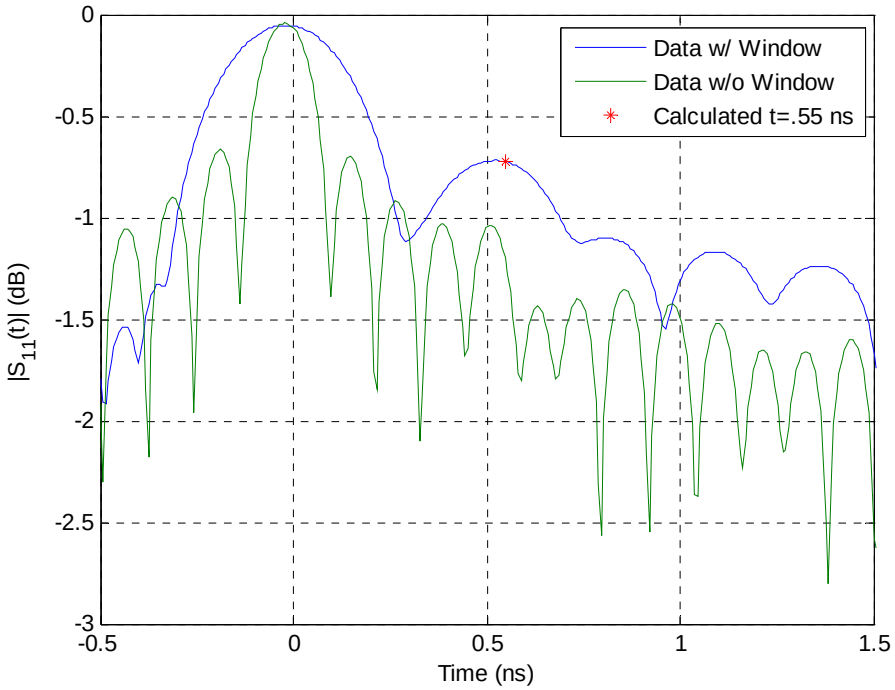

Figure 22: Time Data with Kaiser window from 4" Circular plate with 4.39mm thick Plexiglas sample

Table 2: Kaiser window edge response times compared with their difference from ideal and corresponding amplitudes

		Time (ns)	Diff. from ideal (ns)	Amplitude
6" Square	**Thick Sample**	0.816519	-0.003442	0.002284
	Thin Sample	0.809599	-0.010362	0.010277
4" Square	**Thick Sample**	0.539733	-0.006836	0.005807
	Thin Sample	0.532813	-0.013756	0.011578
1.5" Square	**Thick Sample**	0.207590	0.002559	0.041350
	Thin Sample	0.214509	0.009478	0.045090
6" Circular	**Thick Sample**	0.781921	-0.037933	0.016617
	Thin Sample	0.795760	-0.024094	0.037662
4" Circular	**Thick Sample**	0.518974	-0.027595	0.017445
	Thin Sample	0.518974	-0.027595	0.036518

Blackman-Harris Windowing

This second window option has the advantage that it suppresses the inherent transform domsin sidelobes so that the lower level signal sidelobes can be observed. However, the disadvantage with this window is that the main lobe is wide, leading to reduction resolution (i.e., limits flange size reduction). This may cause a problem when trying to extract the edge response from the 1.5" flange plate because this edge response may be very close to the main lobe. Again, the Blackman Harris window is applied and compared with the unprocessed time domain signal in Figures 23-32. Again, measurements were taken using 6" circular, 4" circular, 6" square, and 4" square, and 1.5" square flange plates.

It is clearly seen that the main lobe is much larger with the Blackman-Harris window. This was a problem when dealing with the measurements for the 1.5" flange plate. The wide main lobe did not allow for an edge response to be seen near the ideal time, instead some sort of multiple of the reflection is most likely seen. Table 3 shows the measured reflections and their difference from the ideal, as well as the amplitudes of

the measured reflections. The Blackman-Harris window is able to isolate a response; however, it proves to be more accurate when the response is further away from the main lobe.

Table 3: Blackman-Harris window edge response times compared with their difference from ideal and corresponding amplitudes

		Time (ns)	Diff. from ideal (ns)	Amplitude
6" Square	**Thick Sample**	0.823439	0.003478	0.003583
	Thin Sample	0.802680	-0.017281	0.008440
4" Square	**Thick Sample**	0.518974	-0.027595	0.004403
	Thin Sample	0.512054	-0.034515	0.008920
1.5" Square	**Thick Sample**	0.408259	0.203338	0.004066
	Thin Sample	0.650447	0.445416	0.004438
6" Circular	**Thick Sample**	0.775001	-0.044853	0.013370
	Thin Sample	0.795760	-0.024094	0.031125
4" Circular	**Thick Sample**	0.512054	-0.034515	0.014051
	Thin Sample	0.512054	-0.034515	0.029290

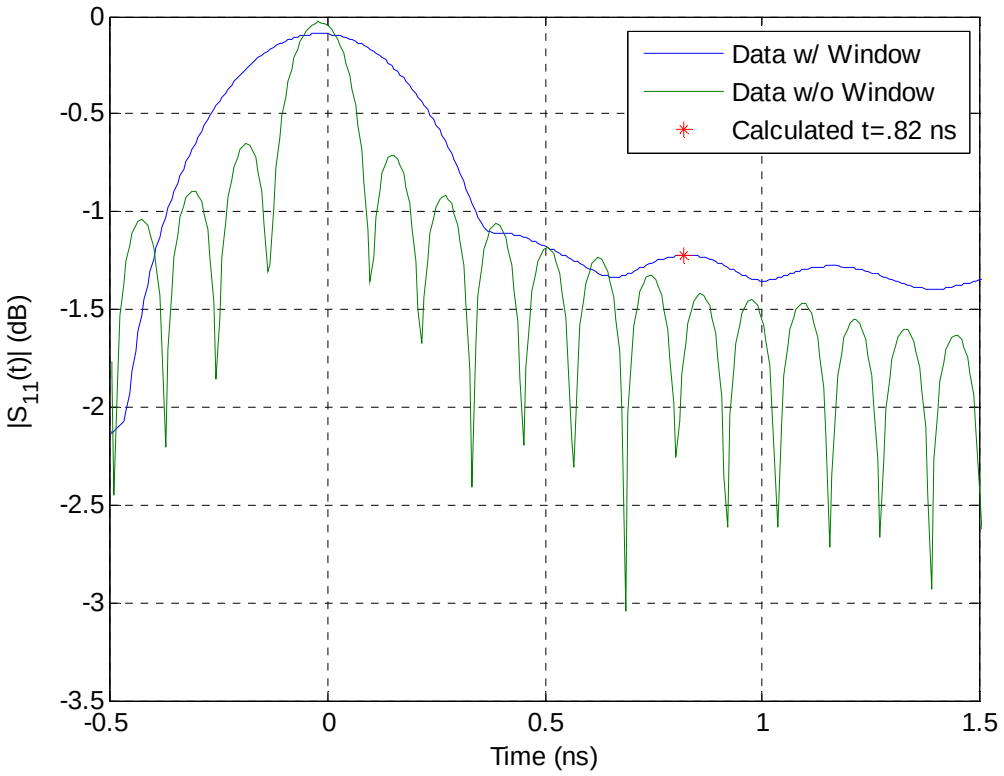

Figure 23: Time Data with Blackman-Harris window from 6" square plate with 5.55mm thick Plexiglas sample

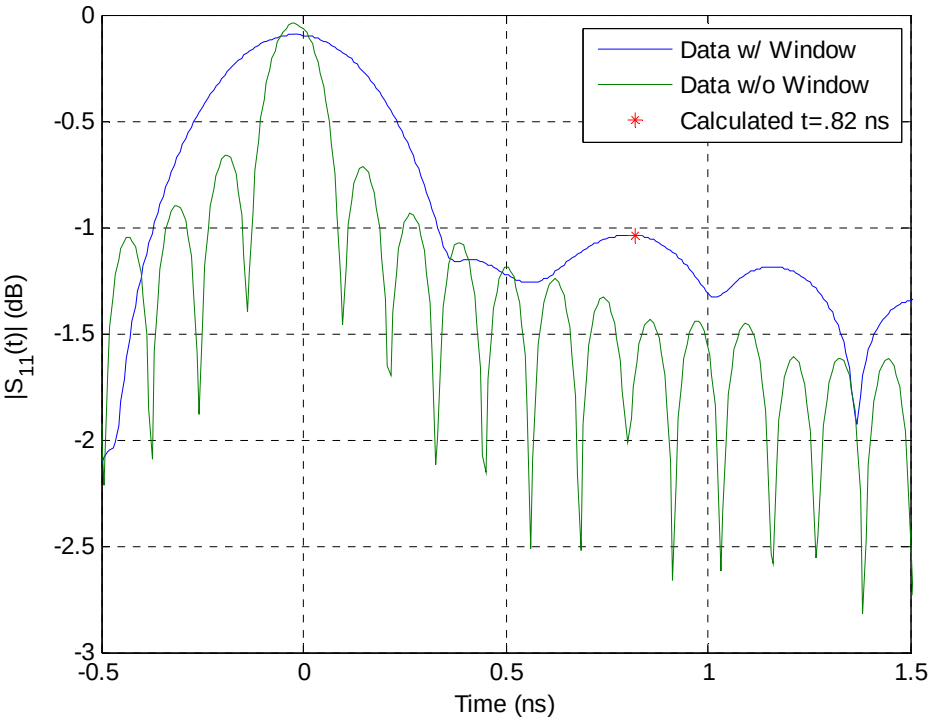

Figure 24: Time Data with Blackman-Harris window from 6" square plate with 4.39mm thick Plexiglas sample

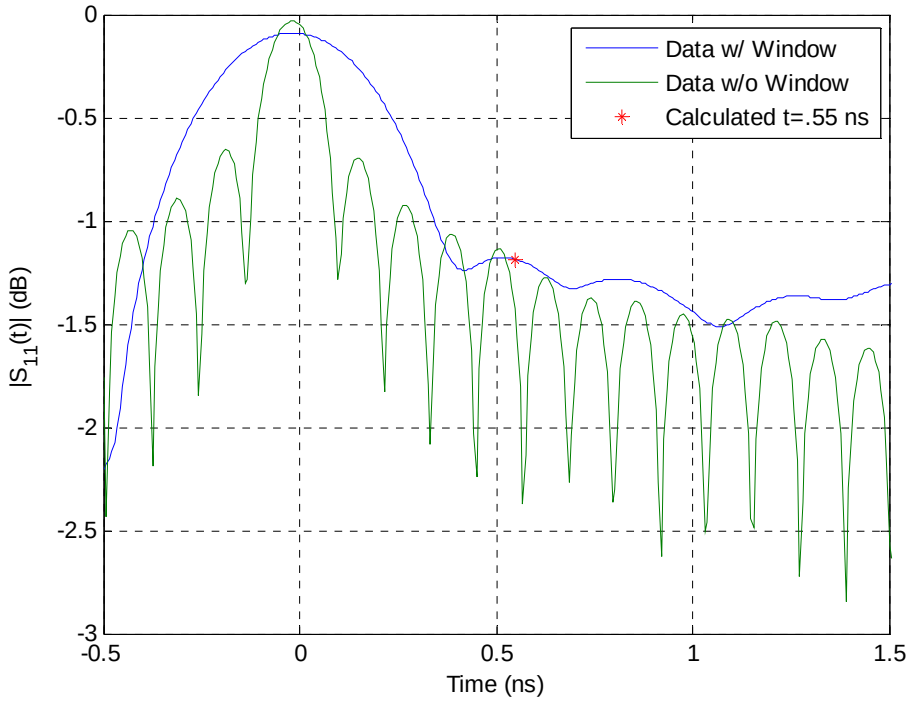

Figure 25: Time Data with Blackman-Harris window from 4" square plate with 5.55mm thick Plexiglas sample

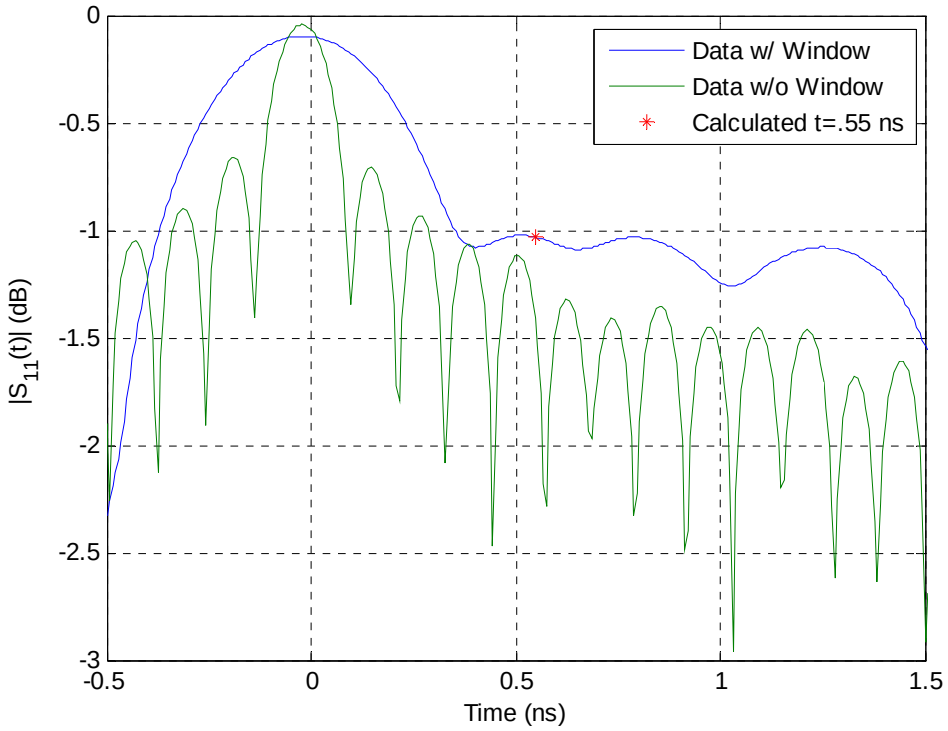

Figure 26: Time Data with Blackman-Harris window from 4" square plate with 4.39mm thick Plexiglas sample

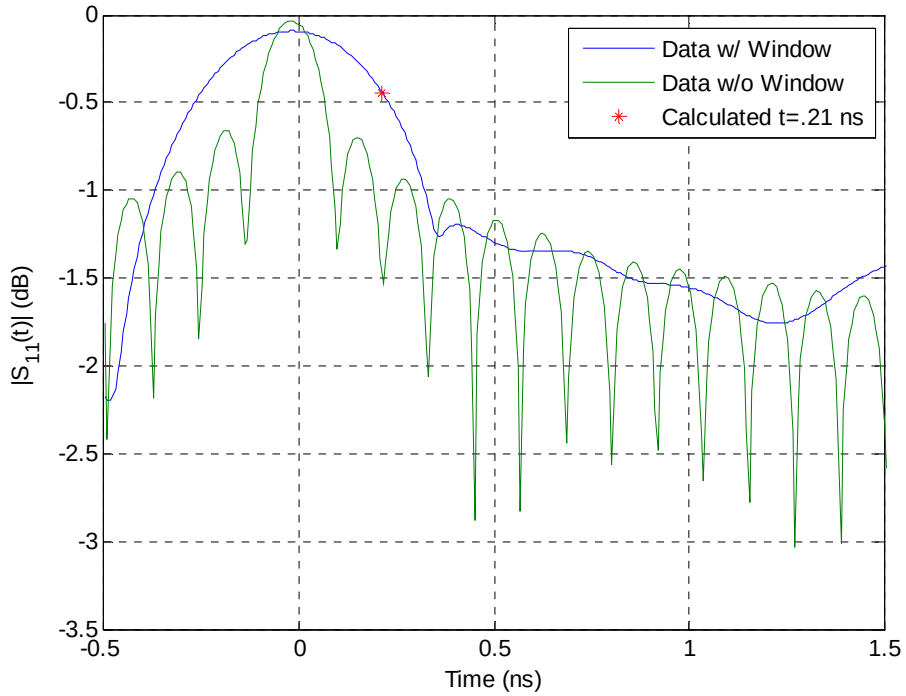

Figure 27: Time Data with Blackman-Harris window from 1.5" square plate with 5.55mm thick Plexiglas sample

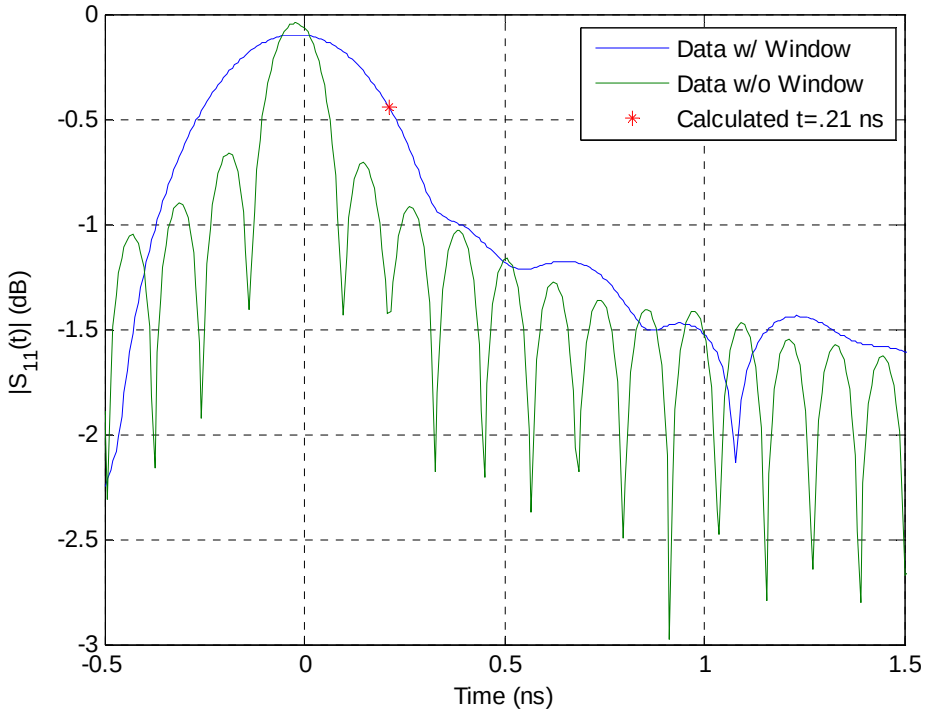

Figure 28: Time Data with Blackman-Harris window from 1.5" square plate with 4.39mm thick Plexiglas sample

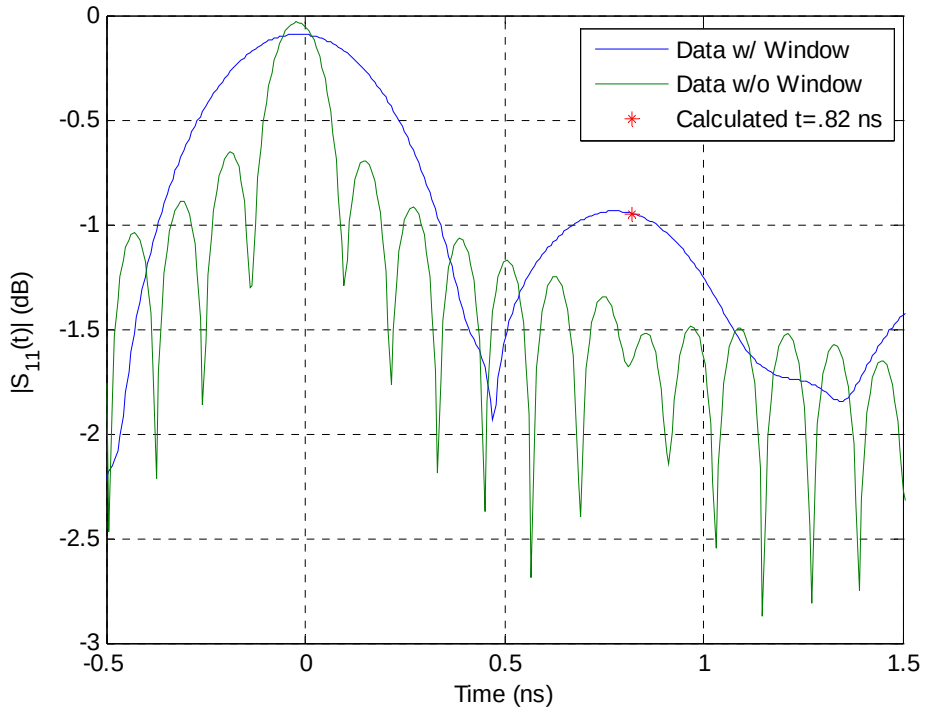

Figure 29: Time Data with Blackman-Harris window from 6" circular plate with 5.55mm thick Plexiglas sample

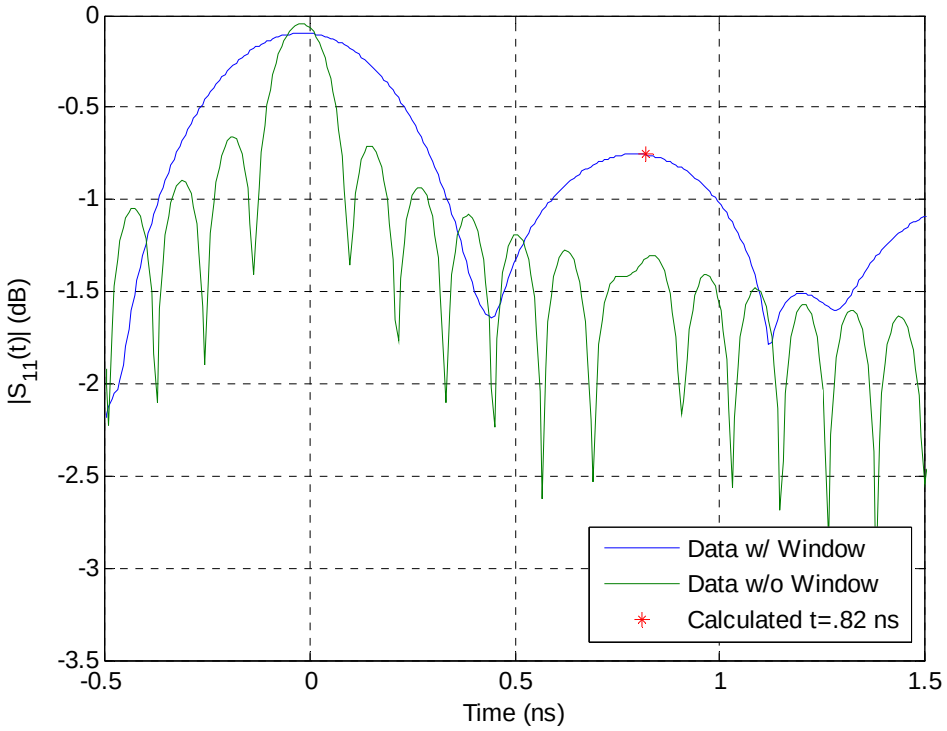

Figure 30: Time Data with Blackman-Harris window from 6" circular plate with 4.39mm thick Plexiglas sample

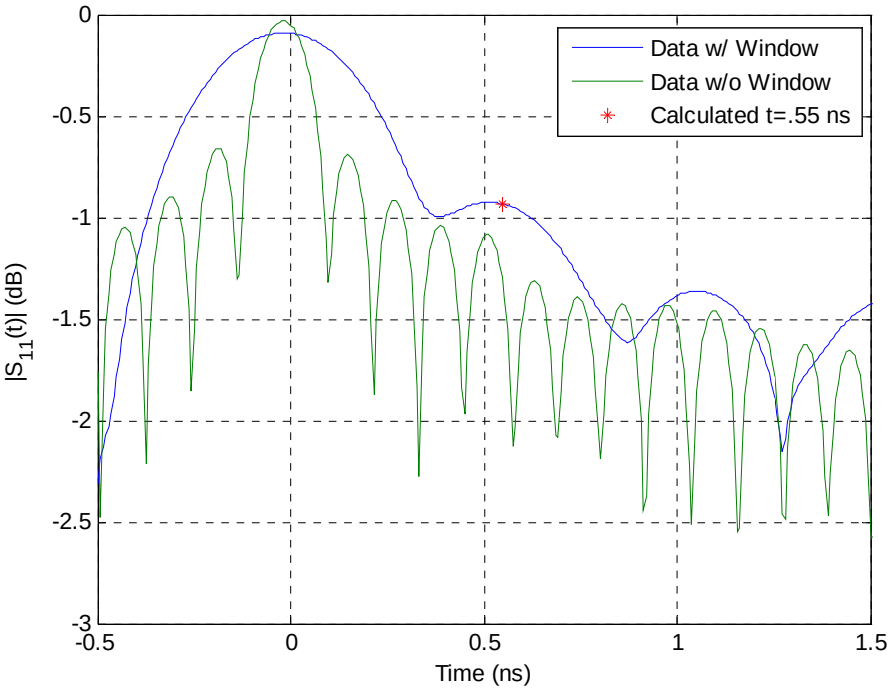

Figure 31: Time Data with Blackman-Harris window from 4" circular plate with 5.55mm thick Plexiglas sample

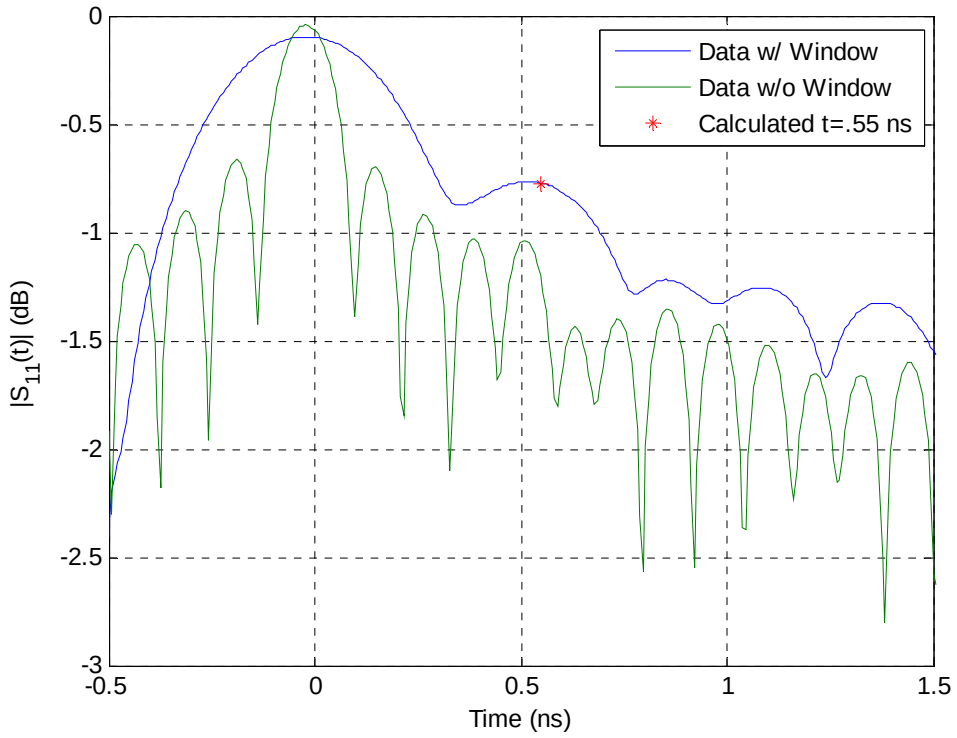

Figure 32: Time Data with Blackman-Harris window from 4" circular plate with 4.39mm thick Plexiglas sample

Complex Permittivity Extraction

Given that the edge reflections have been observed using one of the two signal processing windows, the data can be used to calculate the relative complex permittivity for the sample dielectric material. The extracted permittivity can then be compared to industry standard values for ε' and ε''. For Plexiglas, the complex permittivity values are $\varepsilon' = 2.6$ and $\varepsilon'' = 0.0150$. The frequency range used to collect data was from 6.5 GHz to 15 GHz for both thickness of Plexiglas. The waveguide probe used 6" square, 4" square, 1.5" square, 6" circular, and 4" circular flange plates to measure the edge reflection. The sample dielectric material was Plexiglas with thicknesses of 5.55 mm and 4.39 mm.

The equations to extract the approximate relative complex permittivity were given by (28) and (29). The uncertainty for the waveguide probe measurements can be formulated by using (61)

$$\delta\varepsilon' \approx \left(\frac{-2c^2 {t_{2w_0}}^2}{{d_{2w_0}}^3} \right) \delta d + \left(\frac{2c^2 t_{2w_0}}{{d_{2w_0}}^2} \right) \delta t \tag{63}$$

where d_{2w_0} the calculated vale for the distance and t_{2w_0} is the calculated value for the time. Similarly the uncertainty for (29) using (62) is calculated as

$$\delta\varepsilon'' \approx -\frac{2\sqrt{\varepsilon'}\ln(A)}{k_0\left(d_{1_0}^{2w} - d_{2_0}^{2w}\right)^2}\delta d_2^{2w} + \frac{2\sqrt{\varepsilon'}\ln(A)}{k_0\left(d_{2_0}^{2w} - d_{1_0}^{2w}\right)^2}\delta d_1^{2w} - \frac{2\ln(A)}{k_0\sqrt{\varepsilon'}\left(d_{2_0}^{2w} - d_{1_0}^{2w}\right)^2}\delta\varepsilon' \tag{64}$$

Kaiser Windowing

The approximate extraction method is applied on the data with the Kaiser windowing. The uncertainty is plotted with a 95% confidence interval assuming a Gaussian distribution. Since there are 3 different sizes of square flange plates, the ratio A is calculated by taking the ratio of the amplitudes of the 6" and 4" plates and the 4" and 1.5" plates. From Figures 33-38, it can be seen that the values for ε' all fall within two standard deviations of the extracted data. ε'', however, does not fall within these confidence intervals.

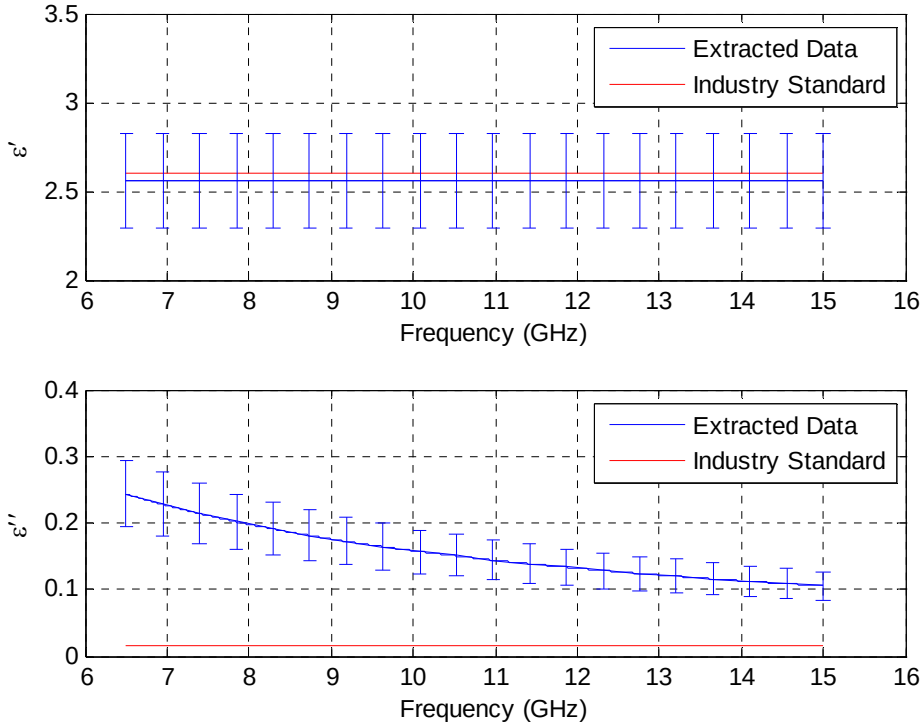

Figure 33: Relative complex permittivity of 5.55 mm thick Plexiglas sample with Kaiser Windowing using 6” and 4” square flange plates

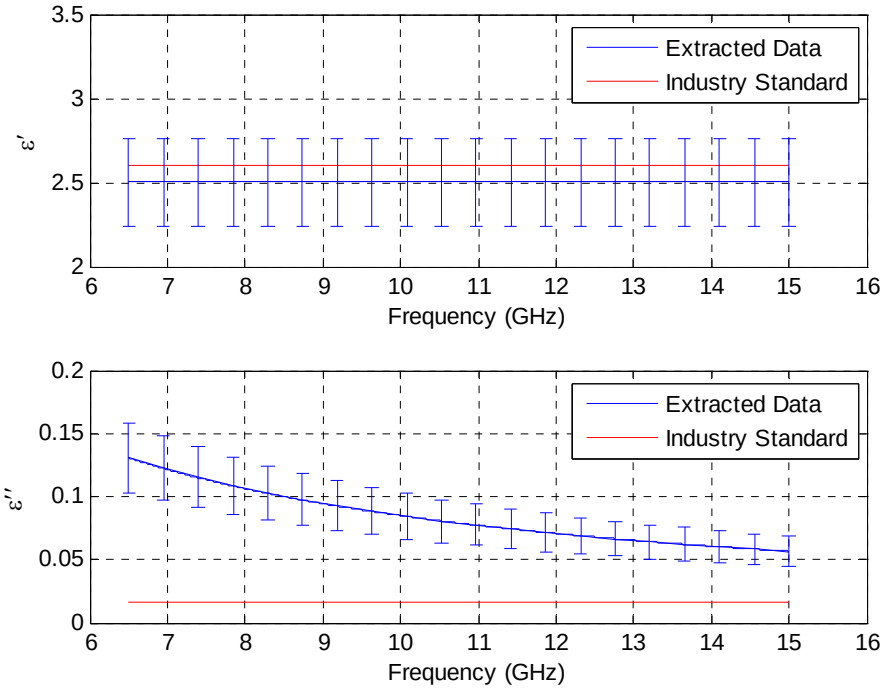

Figure 34: Relative complex permittivity of 4.39 mm thick Plexiglas sample with Kaiser Windowing using 6” and 4” square flange plates

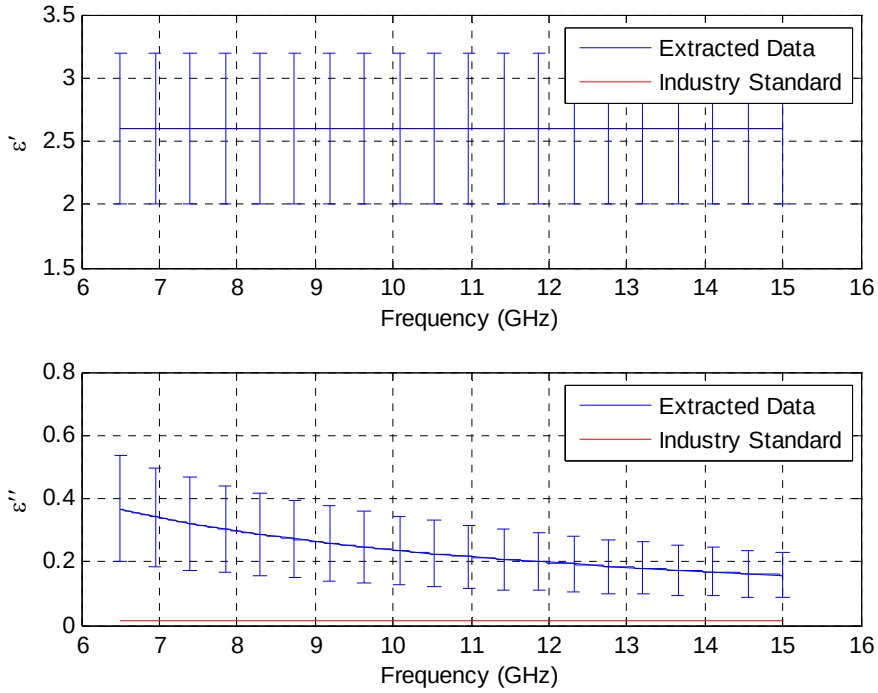

Figure 35: Relative complex permittivity of 5.55 mm thick Plexiglas sample with Kaiser Windowing using 4" and 1.5" square flange plates

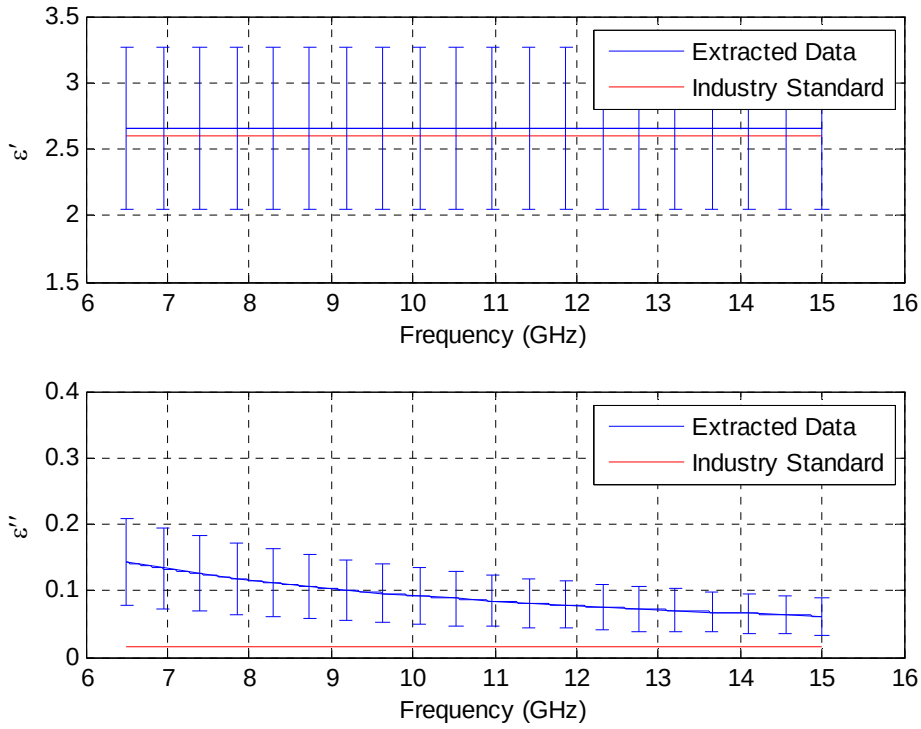

Figure 36: Relative complex permittivity of 4.39 mm thick Plexiglas sample with Kaiser Windowing using 4" and 1.5" square flange plates

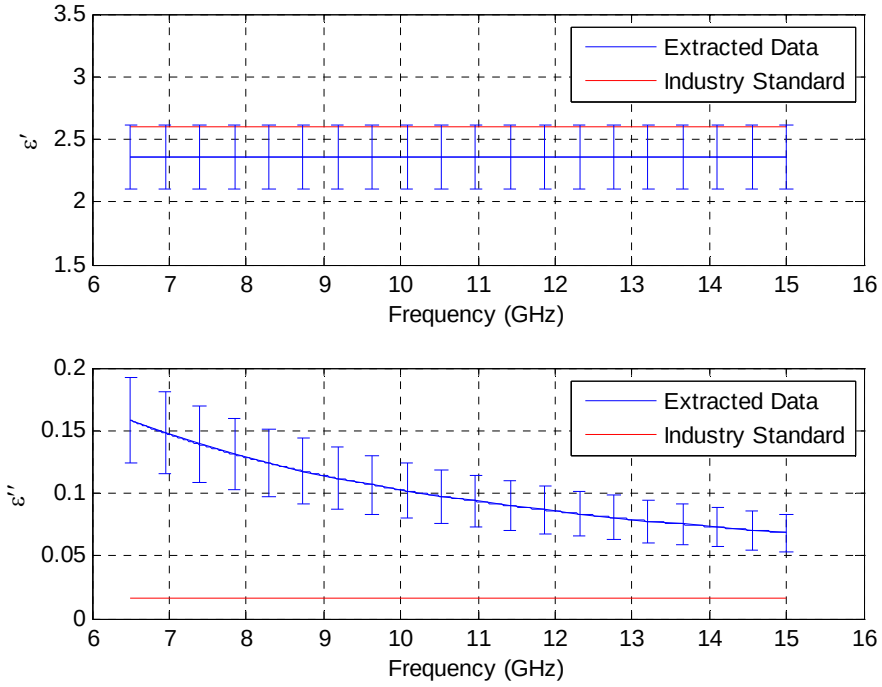

Figure 37: Relative complex permittivity of 5.55 mm thick Plexiglas sample with Kaiser Windowing using 6” and 4” circular flange plates

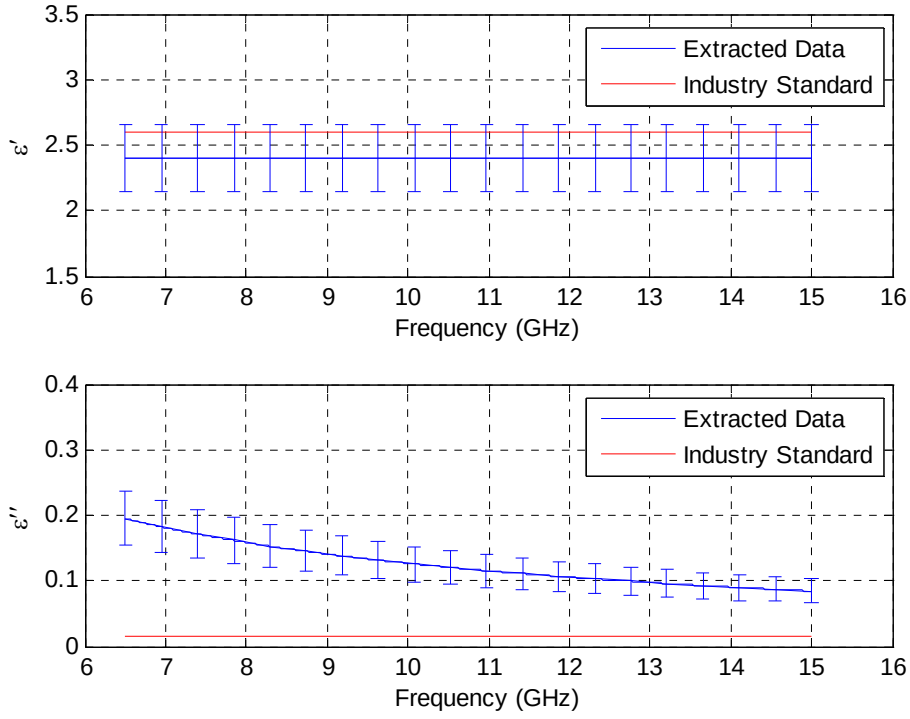

Figure 38: Relative complex permittivity of 4.39 mm thick Plexiglas sample with Kaiser Windowing using 6” and 4” circular flange plates

Blackman-Harris Windowing

Again, the approximate relative permittivity extraction method is applied on the data with Blackman-Harris windowing. The extraction is performed similarly to that of the previous section. The Blackman-Harris windowing has a wider main lobe which may make the resulting data lie outside the 95% confidence intervals. The ratio A is once again calculated by taking the ratio of the amplitudes of the 6" and 4" square flange plates and the 4" and 1.5" square flange plates.

Figures 39-44 show the results of the approximate extraction method. It can be seen that the real part of the permittivity falls within the confidence intervals for the majority of square flange plates. Since the measurements in the time domain did not accurately capture the edge response of the 1.5" square flange plate, the extracted permittivity is an order of magnitude larger.

The assumption that the material under test is a low loss dielectric makes it tolerable to have the imaginary part of ε_r several multiples of the standard industry value. Depending on the application of the dielectric material, the relative complex permittivity may be suitable for use. From the results, it appears that the rectangular flanges are slightly more accurate than the circular flange plates. Table 4 contains all the averaged ε' and ε'' extracted values from both windowing methods.

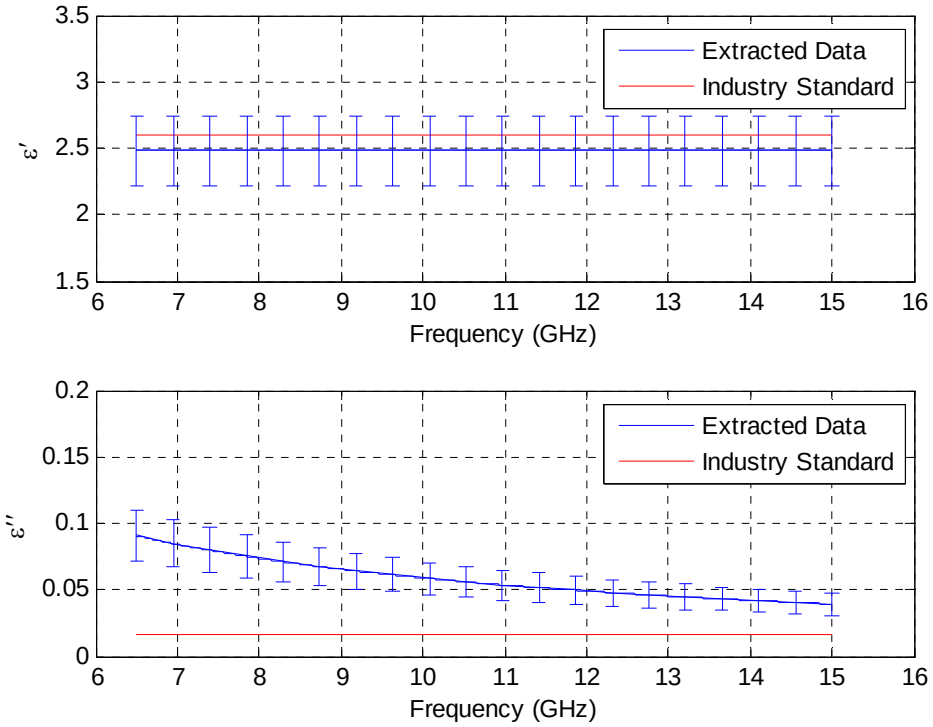

Figure 39: Relative complex permittivity of 5.55 mm thick Plexiglas sample with Blackman-Harris Windowing using 6" and 4" square flange plates

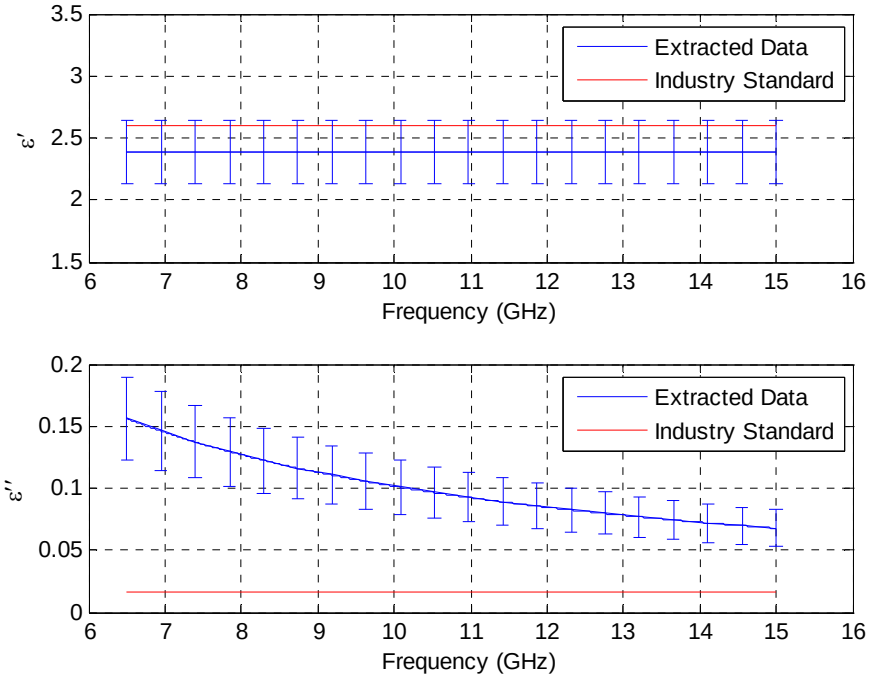

Figure 40: Relative complex permittivity of 4.39 mm thick Plexiglas sample with Blackman-Harris Windowing using 6" and 4" square flange plates

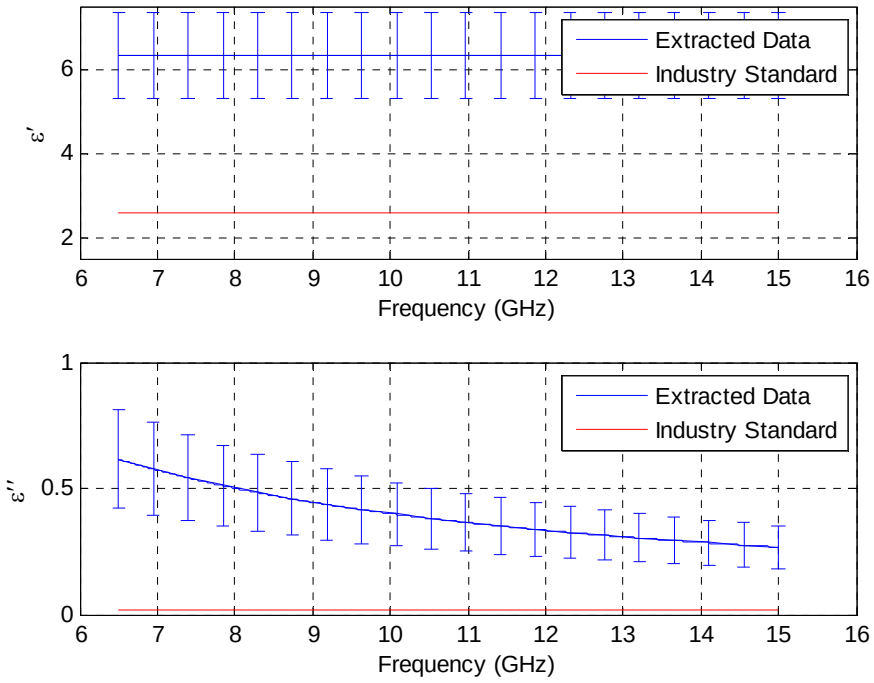

Figure 41: Relative complex permittivity of 5.55 mm thick Plexiglas sample with Blackman-Harris Windowing using 4" and 1.5" square flange plates

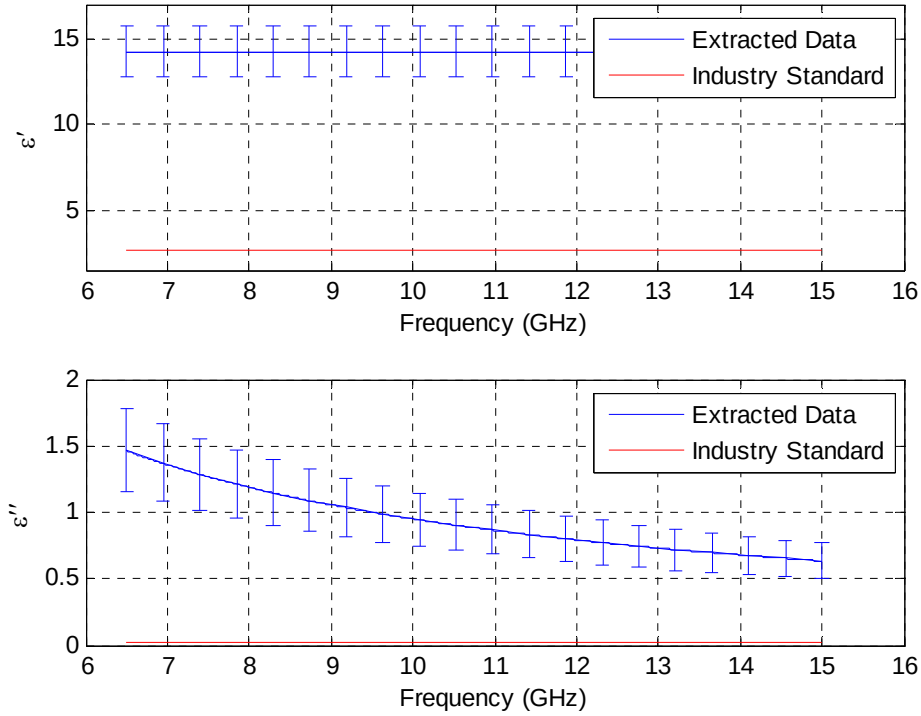

Figure 42: Relative complex permittivity of 4.39 mm thick Plexiglas sample with Blackman-Harris Windowing using 4" and 1.5" square flange plates

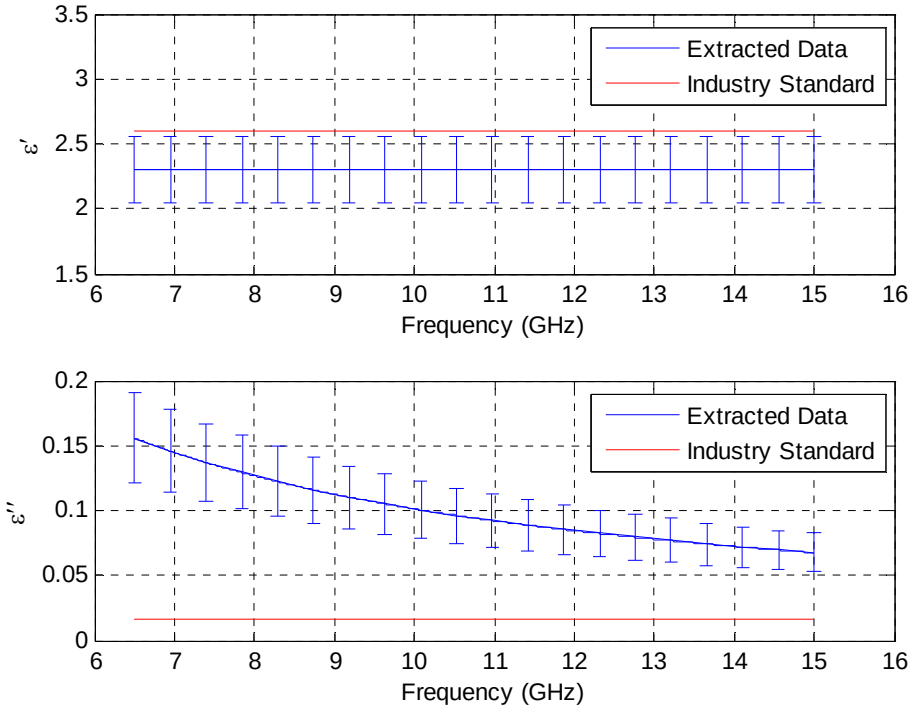

Figure 43: Relative complex permittivity of 5.55 mm thick Plexiglas sample with Blackman-Harris Windowing using 6" and 4" circular flange plates

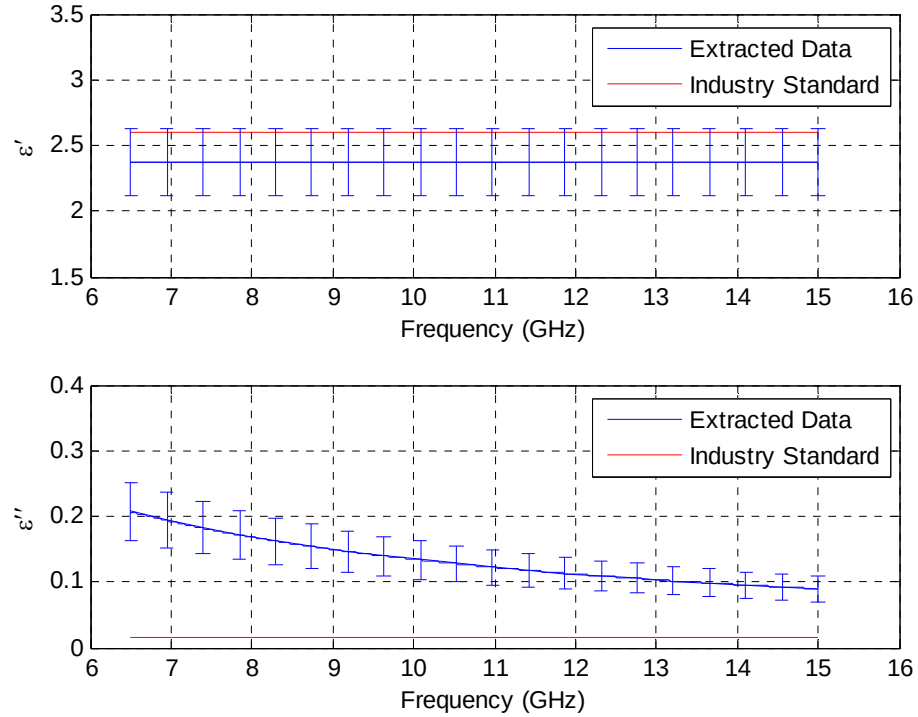

Figure 44: Relative complex permittivity of 4.39 mm thick Plexiglas sample with Blackman-Harris Windowing using 6" and 4" circular flange plates

Table 4: All averaged ε' and ε'' from each measurement with processing window and industry standard values

Applied Window	Flange Plate	Sample Thickness	Avg. ε'	Avg. ε''	Std. ε'	Std. ε''
Kaiser	6"/4" Square	5.55 mm	2.5566	0.1558	2.6	0.015
		4.39 mm	2.5026	0.0837	2.6	0.015
	4"/1.5" Square	5.55 mm	2.6004	0.2342	2.6	0.015
		4.39 mm	2.6584	0.0913	2.6	0.015
	Circular	5.55 mm	2.3545	0.1012	2.6	0.015
		4.39 mm	2.3968	0.1248	2.6	0.015
Blackman-Harris	6"/4" Square	5.55 mm	2.4830	0.0581	2.6	0.015
		4.39 mm	2.3867	0.0999	2.6	0.015
	4"/1.5" Square	5.55 mm	6.3269	0.3943	2.6	0.015
		4.39 mm	14.226	0.9360	2.6	0.015
	Circular	5.55 mm	2.3027	0.0998	2.6	0.015
		4.39 mm	2.3657	0.1325	2.6	0.015

Summary

Chapter 4 provided the results of a simple relative complex permittivity extraction technique using two different signal processing windows. This technique takes advantage of the edge reflections from the parallel-plate region creating by the dual ridged waveguide probe. By using the calibration and frequency range details in Chapter 3, measurements were taken to show the response and then extract the relative complex permittivity based on the frequency data collected. The uncertainty of the measurements was accounted for and incorporated into the results. The frequency range covered in the measurements was 6.5 GHz to 15 GHz. There were two Plexiglas samples used as a low loss dielectric material. Their thicknesses were 5.55 mm and 4.39 mm. There were a total of 3 different sized probes used for measurement. A dual ridged waveguide was attached to 6 inch, 4 inch, and 1.5 inch square plates. Then measurements were taken using 6 inch and 4 inch diameter circular flange plates. The result of using windowing functions showed that the Kaiser window provided more accurate results. It was found

that the main lobe of the Blackman-Harris window was too wide to solicit a reflection when using the 1.5 inch square plate. When the final relative complex permittivity values were extracted, the square flange plates had slightly more accurate values than the circular flange plates. The largest factor for uncertainty is the temporal resolution, which in turn signifies that the bandwidth of the system was reduced. In order to extract more accurate values, the bandwidth of the system needs to be increased. This may be achieved via the use of a suitable suite of dual ridged waveguide calibration standards and suppression of higher-order parallel-plate modes.

V. Conclusions and Future Work

A simple and approximate method has been applied and modified in order to extract the relative complex permittivity from a low loss, non-magnetic, non-dispersive dielectric material. The method was adapted to take measurements with a dual ridged waveguide probe. The sample material used in this research is Plexiglas. It was used to verify that this computationally simple method can provide fairly accurate results. However, this method can be used to extract these parameters out of other materials that adhere to the limitations. The greatest benefit of this method is that it is computationally simple and non-destructive. Although other non-destructive methods exist, this method is orders of magnitude faster to solve. Since this method is non-destructive, it is not necessary to spend time machining the sample to fit a holder nor are there errors from the placement of the material in a holder. Once measurements are taken of the material, all the data can be processed and subsequently analyzed.

Conclusions

Although the prior simple extraction technique [12] used a rectangular waveguide probe, it is shown in this research that a dual ridged waveguide can also be used to take accurate measurements. The advantage of the dual ridged waveguide is the increased bandwidth available for measurements thus leading to flange size reduction and probe agility. The method was also altered to use two signal processing windows in the time domain data. This simple method is modular, which gives it the advantage of being able to be changed at the various processing steps.

Plate Geometry

The results of Chapter 4 show that there is no major significance in the chosen plate geometry. However, it is shown that the smaller plate sizes have a noticeably better accuracy. This may be due to the fact that more of the edge response is able to reflect back into the dual ridged waveguide instead of propagating into free space. Also, there are noticeable 2nd and 3rd order reflections, however, this cannot be known in advance since the dielectric material is assumed to be unknown in general.

Signal Processing

The final extracted data does show that the Kaiser windowed data provided more accurate values than the Blackman-Harris windowed data. The Blackman-Harris window has a wider main lobe than the Kaiser window, which makes the edge response harder to distinguish. This is evident in the 1.5" square flange plate measurements. The Kaiser windowing provides overall more accurate data that is still within the confidence intervals for ε'. The imaginary part of the relative complex permittivity relies on the ratio of two different dimension flange plates, which may be a cause of why ε'' did not fall into the 95% confidence interval.

Frequency Range

The major factor in the uncertainty analysis was the temporal resolution. This is inversely proportional to the bandwidth used for measurement in the system. By taking advantage of the full frequency range available in the dual ridged waveguide, it would be possible to reduce the uncertainty of the measurements. Another factor is the frequency limitations of the NWA. Although the NWA measures data up to 20 GHz, it may be

possible to use a waveguide that can provide an even larger bandwidth while still being able to transmit the edge reflection.

Future Research

The largest factor needed to improve the uncertainty of the measurement is the bandwidth. The WRD650 waveguide has a bandwidth of 6.5 GHz to 18 GHz, however, a high end frequency of 15 GHz was used because of calibration constraints. One area for future work is to obtain flange plates with the proper thickness in order to facilitate the 3 short method calibration to the maximum bandwidth of the dual ridged waveguide. Another possibility is to machine a line standard or multiple line standards to facilitate the calibration of the probe in a full two port calibration. Although, two different windows were used, there are a plethora of signal processing windows, which might be able to bring out the edge response even more clearly, leading to enhanced accuracy. The last suggestion for future work is to try different size and shapes of flange plates in order to obtain a more prominent edge reflection in the parallel-plate region.

Bibliography

[1] A. Leon-Garcia, *Probability, Statistics, and Random Processes for Electrical Engineering*, 3rd Ed. Upper Saddle River, NJ: Pearson Education, Inc, 2008.

[2] Agilent Technologies, "Agilent PNA Series Network Analyzer," Printed Version of PNA Help User's and Programming Guide, June 2010.

[3] C. A. Balanis, *Advanced Engineering Electromagnetics*, New York: Wiley & Sons, 1989.

[4] F. J. Harris, "On the Use of Windows for Harmonic Analysis with the Discrete Fourier Transform," IEEE Proceedings, volume 66, 51-83. Jan 1978.

[5] J. P. Montgomery, "On the Complete Eigenvalue Solution of Ridged Waveguide," IEEE Transactions on Microwave Theory and Techniques, volume MTT-19, 547-555 June 1971.

[6] L. F. Chen, C. K. Ong, C. P. Neo, V. V. Varadan, and V. K. Varadan, *Microwave Electronics Measurement and Materials Characterization*, New York: John Wiley & Sons, 2004.

[7] M. W. Hyde et al., "Nondestructive electromagnetic material characterization using a dual waveguide probe: A full wave solution," *Radio Sci*., 44, RS3013.

[8] R. E. Collin, *Field Theory of Guided Waves*, 2nd Ed., Piscataway, N.J., IEEE Press, 1991

[9] R. F. Harrington, *Time-Harmonic Electromagnetic Fields*, New York: IEEE Press, 2001.

[10] S. Haykin and B. Van Veen, *Signals and Systems*, 2nd Ed. New York: John Wiley & Sons, 2003.

[11] S. P. Dorey, "Stepped waveguide electromagnetic material characterization technique," M.S. Thesis, Air Force Institute of Technology, Wright-Patterson Air Force Base, Ohio, 2004.

[12] T. S. Olney, "A simple non-destructive method for characterizing non-dispersive, low-loss dielectrics," M.S. Thesis, Air Force Institute of Technology, Wright-Patterson Air Force Base, Ohio, 2011

REPORT DOCUMENTATION PAGE

Form Approved
OMB No. 074-0188

1. REPORT DATE *(DD-MM-YYYY)*	2. REPORT TYPE	3. DATES COVERED *(From – To)*
22-03-2012	Master's Thesis	Sept 2010-Mar 2012

4. TITLE AND SUBTITLE
A High Bandwidth Non-Destructive Method for Characterizing Simple Media

5a. CONTRACT NUMBER

5b. GRANT NUMBER

5c. PROGRAM ELEMENT NUMBER

6. AUTHOR(S)
Szuster, Matthew L., Second Lieutenant, USAF

5d. PROJECT NUMBER
JON# 12G170

5e. TASK NUMBER

5f. WORK UNIT NUMBER

7. PERFORMING ORGANIZATION NAMES(S) AND ADDRESS(S)
Air Force Institute of Technology
Graduate School of Engineering and Management (AFIT/ENG)
2950 Hobson Way, Building 640
WPAFB OH 45433-8865

8. PERFORMING ORGANIZATION REPORT NUMBER
AFIT/GE/ENG/12-39

9. SPONSORING/MONITORING AGENCY NAME(S) AND ADDRESS(ES)
Air Force Research Lab
Mr. Garrett Stenholm
2591 K Street, Bldg. 254
Wright-Patterson AFB, OH 45433-7602
(937) 255-9179, Garrett.Stenholm@wpafb.af.mil

10. SPONSOR/MONITOR'S ACRONYM(S)
AFRL/RYS

11. SPONSOR/MONITOR'S REPORT NUMBER(S)

12. DISTRIBUTION/AVAILABILITY STATEMENT
Approved for public release; distribution unlimited

13. SUPPLEMENTARY NOTES

14. ABSTRACT
The relative complex permittivity can be extracted with time domain data from a perfect electrical conductor (PEC) backed sample of a low-loss, non-dispersive dielectric using dual ridged waveguide aperture probes with attached PEC flange plates of the same geometry and different dimensions. The temporal domain measurement of interest is the ability to detect the reflection from the edge of the flange plate in the parallel region created by the flange plate and the PEC backing on the dielectric sample. Signal processing windows are applied to the data in order to exploit this edge reflection. The types of signal processing methods used and the geometry and size of the flange plate help identify the edge reflection. Measurements are taken using square and circular flange plates of different dimensions. Measured data is then processing using Kaiser and Blackman-Harris windows to show the edge reflection. A simple extraction technique for the permittivity is used and compared with industry standard values.

15. SUBJECT TERMS
Dual Ridged Waveguide, Material Measurement, Permittivity, Dielectric

16. SECURITY CLASSIFICATION OF:			17. LIMITATION OF ABSTRACT	18. NUMBER OF PAGES	19a. NAME OF RESPONSIBLE PERSON
a. REPORT	b. ABSTRACT	c. THIS PAGE			Dr. Michael Havrilla
U	U	U	UU	74	19b. TELEPHONE NUMBER *(Include area code)* (937) 255-6565, x 4582 (Michael.Havrilla@afit.edu)